ORNL/TM-8861
Dist. Category UC-20

FUSION ENERGY DIVISION

STEEPEST DESCENT MOMENT METHOD FOR THREE-DIMENSIONAL MAGNETOHYDRODYNAMIC EQUILIBRIA

S. P. Hirshman
Fusion Energy Division

J. C. Whitson
UCC-ND Computer Sciences

Date Published - November 1983

Prepared by the
OAK RIDGE NATIONAL LABORATORY
Oak Ridge, Tennessee 37830
operated by
UNION CARBIDE CORPORATION
for the
U.S. DEPARTMENT OF ENERGY
under Contract No. W-7405-eng-26

CONTENTS

ABSTRACT

An energy principle is used to obtain the solution of the magnetohydrodynamic (MHD) equilibrium equation $\vec{J} \times \vec{B} - \nabla p = 0$ for nested magnetic flux surfaces that are expressed in the inverse coordinate representation $\mathcal{R} = \mathcal{R}(\rho,\theta,\zeta)$. Here, θ and ζ are poloidal and toroidal flux coordinate angles, respectively, and $p = p(\rho)$ labels a magnetic surface. Ordinary differential equations in ρ are obtained for the Fourier amplitudes (moments) in the doubly periodic spectral decomposition of $\mathcal{R}$. A steepest descent iteration is developed for efficiently solving these nonlinear, coupled moment equations. The existence of a positive-definite energy functional guarantees the monotonic convergence of this iteration toward an equilibrium solution (in the absence of magnetic island formation). A renormalization parameter λ is introduced to ensure the rapid convergence of the Fourier series for $\mathcal{R}$, while simultaneously satisfying the MHD requirement that magnetic field lines are straight in flux coordinates. A descent iteration is also developed for determining the self-consistent value for λ.

I. INTRODUCTION

The global analysis of finite-aspect-ratio, high-beta, three-dimensional (3-D) toroidal configurations with complex external coil configurations of the type envisioned for fusion reactor applications generally requires numerical methods. The variational formulation of MHD equilibria[1,2] provides a mathematically efficient prescription for treating the truncation or closure of an approximate finite-series solution of the nonlinear equilibrium equations. Also inherent in any energy principle is an iteration scheme for obtaining the solution of this truncated set of equations, which is based on seeking the minimum energy state.

The practical application of variational principles for obtaining numerical equilibria has progressed recently, so that there are currently fully 3-D codes based on either Eulerian[3] or Lagrangian[4] formulations. Both of these methods are numerically inefficient in comparison with moment methods that have been applied to two-dimensional (2-D) problems arising in systems with an ignorable spatial coordinate[5] or that result from averaging 3-D equilibria.[6] This has prompted the present formulation of 3-D moment equilibria, as well as an alternate approach[7] based on the variational principle of Grad.[2]

The moment expansion of the plasma equilibrium results in a finite set of coupled, nonlinear, ordinary differential equations for the Fourier amplitudes of the inverse mapping[8] $\vec{x} = \vec{x}(\rho,\theta,\zeta)$, where (ρ,θ,ζ) are flux coordinates, ρ labels the flux surfaces (constant pressure contours), and θ and ζ are poloidal and toroidal angle variables, respectively. In the present paper, a steepest descent procedure is developed for solving the

nonlinear moment equations that arise in MHD equilibrium problems. This is the Fourier space formulation of the numerical scheme used in Ref. 4.

The success of moment methods is attributable in part to the rapid convergence of the Fourier series for the inverse equilibrium coordinates. In the present formulation, this convergence property is ensured by introducing a renormalization parameter (Sec. II) to distinguish between the geometric and the magnetic poloidal angles (the latter describes straight magnetic field lines).

The MHD energy principle[1] is used in Sec. III to obtain the equilibrium equations in a conservative form. It is shown that the variational moment equations correspond to the spectral coefficients of the covariant components of the MHD force. In Sec. IV, the Fourier decomposition of the inverse mapping is introduced, and the steepest descent method of solution for the moment amplitudes is derived. The boundary conditions at the magnetic axis and at the plasma boundary are discussed in Sec. V, and the descent algorithm is generalized to include a vacuum region surrounding the plasma. A geometric interpretation of the moment representation in three dimensions is given in Sec. VI. The moment solution of an exact 2-D equilibrium is discussed in Sec. VII to clarify the role of the poloidal angle θ. Some details of the numerical techniques used to solve the inverse equations are given in Sec. VIII. A Galerkin method for treating the magnetic axis and plasma shift is described in Sec. IX, and some numerical results are presented in Sec. X.

The equilibria calculated here have a single magnetic axis. By applying magnetic perturbations of the form $\vec{B} = \nabla \times A_{\parallel}\vec{B}_0$, where $A_{\parallel} = \sum_{m,n} A_{mn}(\rho)\exp[i(m\theta - n\zeta)]$, it is possible to investigate the stability of these equilibria to a more general class of (tearing) perturbations.

II. EQUILIBRIUM EQUATIONS IN FLUX COORDINATES

The equations describing MHD equilibrium of a static (no fluid flow), isotropic plasma are the force balance equation and Ampère's and Gauss's laws:

$$\vec{F} \equiv -\vec{J} \times \vec{B} + \nabla p = 0 \ , \tag{1a}$$

$$\nabla \times \vec{B} = \mu_0 \vec{J} \ , \tag{1b}$$

$$\nabla \cdot \vec{B} = 0 \ , \tag{1c}$$

where $p = p(\rho)$ is the pressure and ρ is a radial coordinate labeling a magnetic flux surface. The quantity $\vec{F}$ is the residual MHD force, which must vanish in equilibrium. For the nested toroidal flux surface geometry considered here, flux coordinate angles θ and ζ may be introduced, where θ is a poloidal angle ($\Delta\theta = 2\pi$ once the short way around the magnetic axis) and ζ is a toroidal angle ($\Delta\zeta = 2\pi$ once the long way around the torus). The conditions $\vec{B} \cdot \nabla p = 0$ and $\nabla \cdot \vec{B} = 0$ can be satisfied by writing $\vec{B}$ in contravariant form as follows:[1]

$$\begin{aligned} \vec{B} &= \nabla\zeta \times \nabla\chi + \nabla\Phi \times \nabla\theta^* \\ &= B^{\theta}\vec{e}_{\theta} + B^{\zeta}\vec{e}_{\zeta} \ , \end{aligned} \tag{2}$$

where $2\pi\chi(\rho)$ and $2\pi\Phi(\rho)$ are, respectively, the poloidal and toroidal magnetic fluxes enclosed between the magnetic surface labeled ρ and the magnetic axis ($\rho = 0$, where $\nabla\chi = 0$),

$$\theta^* = \theta + \lambda(\rho,\theta,\zeta) \tag{3a}$$

is the poloidal angle that makes the magnetic field lines straight[9] [i.e., the local rotation number $\vec{B} \cdot \nabla\theta^* / \vec{B} \cdot \nabla\zeta$ is a function of ρ alone in the (ρ,θ^*,ζ) coordinate system], and λ is a periodic function of θ and ζ with zero average over a magnetic surface, $\iint d\theta\, d\zeta\, \lambda = 0$. The contravariant basis vectors are $\vec{e}^i \equiv \nabla\alpha_i$, where $\vec{\alpha} = (\rho,\theta,\zeta)$, and the covariant basis vectors are $\vec{e}_i \equiv \partial\vec{x}/\partial\alpha_i = \sqrt{g}\vec{e}^j \times \vec{e}^k$, where (i,j,k) forms a positive triplet and $\sqrt{g} = (\nabla\rho \cdot \nabla\theta \times \nabla\zeta)^{-1}$ is the Jacobian. Thus, from Eq. (2), the contravariant components of the magnetic field are $B^i \equiv \vec{B} \cdot \vec{e}^i$, where

$$B^\theta = \frac{1}{\sqrt{g}} \left(\chi' - \Phi' \frac{\partial\lambda}{\partial\zeta}\right) \quad , \tag{3b}$$

$$B^\zeta = \frac{1}{\sqrt{g}} \Phi' \left(1 + \frac{\partial\lambda}{\partial\theta}\right) \quad , \tag{3c}$$

$B^\rho = 0$, and the prime denotes $\partial/\partial\rho$. The covariant components $B_i \equiv \vec{B} \cdot \vec{e}_i$ are related to B^i through the metric tensor $g_{ij} \equiv \vec{e}_i \cdot \vec{e}_j$:

$$B_i = B^\theta g_{\theta i} + B^\zeta g_{\zeta i} \quad , \tag{3d}$$

as can be verified by taking the scalar product of Eq. (2) with $\vec{e}_i$.

Although the function $\lambda(\rho,\theta,\zeta)$ in Eq. (3a) can be eliminated[9] by taking $\theta = \theta^*$, its retention here provides flexibility in specifying the poloidal angle θ. The role of the poloidal angle in the moment expansion of equilibria is to yield rapidly convergent[5] Fourier series for the spatial coordinates $\vec{x}(\rho,\theta,\zeta)$. Since only truncated series are used in practice, a proper choice for θ is necessary to provide adequate accuracy in the approximate moment solution. In general, this value for θ is incompatible with the requirement that magnetic field lines are straight in

(θ^*,ζ) coordinates. The inclusion of λ therefore generates a convergent resummation of the inverse equilibrium Fourier moment expansion. In this context, λ assumes the role of a renormalization parameter.

Inserting Eq. (2) into Eq. (1a) yields

$$\vec{F} = F_\rho \nabla\rho + F_\beta \vec{\beta} \ , \tag{4a}$$

where

$$F_\rho = \sqrt{g}\left(J^\zeta B^\theta - J^\theta B^\zeta\right) + p' \ , \tag{4b}$$

$$F_\beta = J^\rho \ , \tag{4c}$$

$\vec{\beta} = \sqrt{g}\left(B^\zeta \nabla\theta - B^\theta \nabla\zeta\right)$ and $J^i \equiv \vec{J} \cdot \nabla\alpha_i = \mu_0^{-1} \nabla \cdot \left(\vec{B} \times \nabla\alpha_i\right)$. There are only two independent components of $\vec{F}$, since the component $\vec{B} \cdot \vec{F} = p'\vec{B} \cdot \nabla\rho = 0$ is already incorporated into the representation of $\vec{B}$ in Eq. (2). Writing J^i in terms of the covariant components of $\vec{B}$ yields expressions for the forces in terms of the flux functions, χ', Φ', and p', and the metric:

$$F_\rho = \mu_0^{-1}\left(B^\theta \frac{\partial B_\theta}{\partial\rho} + B^\zeta \frac{\partial B_\zeta}{\partial\rho} - \vec{B} \cdot \nabla B_\rho\right) + p' \ , \tag{4d}$$

$$F_\beta = \frac{1}{\mu_0\sqrt{g}}\left(\frac{\partial B_\zeta}{\partial\theta} - \frac{\partial B_\theta}{\partial\zeta}\right) \ . \tag{4e}$$

Here, for any scalar A, the derivative along a magnetic field line is

$$\vec{B} \cdot \nabla A \equiv B^\theta \frac{\partial A}{\partial\theta} + B^\zeta \frac{\partial A}{\partial\zeta} \ . \tag{4f}$$

In the 2-D axisymmetric case,[5,8] $F_\beta = 0$ can be integrated to yield

$$B_\zeta = F(\rho) \quad . \tag{5a}$$

Noting that $g_{\theta\zeta} = g_{\rho\zeta} = 0$ and $\partial\lambda/\partial\zeta = 0$, due to axisymmetry, and $B^\zeta = B_\zeta/g_{\zeta\zeta}$ with $g_{\zeta\zeta} = R^2$ (where R is the major radius, see Fig. 1), Eq. (4d) becomes the inverse Grad-Shafranov equation:

$$F_\rho = \frac{\chi'}{\mu_0\sqrt{g}}\left[\frac{\partial}{\partial\rho}\left(\frac{\chi' g_{\theta\theta}}{\sqrt{g}}\right) - \frac{\partial}{\partial\theta}\left(\frac{\chi' g_{\rho\theta}}{\sqrt{g}}\right)\right] + \frac{FF'}{\mu_0 R^2} + p' \quad . \tag{5b}$$

From Eqs. (3c,d), note that Eq. (5a) can be written $(\Phi' R^2/\sqrt{g})(1 + \partial\lambda/\partial\theta) = F(\rho)$, which yields $\Phi'(\rho) = \langle\sqrt{g}/R^2\rangle F(\rho)$ and

$$\frac{\partial\lambda}{\partial\theta} = \frac{\sqrt{g}/R^2}{\langle\sqrt{g}/R^2\rangle} - 1 \quad . \tag{5c}$$

Here, the angle brackets denote a normalized θ average.

Equation (5c) shows that in 2-D geometry, the straight magnetic field line system for $\lambda = 0$ is one for which $\sqrt{g}/R^2$ is constant on a magnetic surface. Consider an equilibrium that is approximated by shifted, elliptical flux surfaces for which the cylindrical coordinates (R,Z) have the low-order Fourier representation $R = R_0(\rho) + R_1(\rho)\cos\theta$, $Z = Z_1(\rho)\sin\theta$. Analysis[8] of this configuration indicates that to leading order in the inverse aspect ratio, the condition $\partial(R^2/\sqrt{g})/\partial\theta = 0$ in the (ρ,θ) coordinate system leads to an unphysical inward shift $\Delta = R_0(0) - R_0(\rho) \leq 0$ which is independent of the plasma pressure. The retention of λ allows for the surface variation of $\sqrt{g}/R^2$ in the (ρ,θ)

coordinate system, where the low-order Fourier series representation for (R,Z) is appropriate. It also yields the correct variation[5] of $R_0(\rho)$ with pressure. An explicit analytic calculation of λ illustrating this behavior is given in Sec. VII.

III. ENERGY PRINCIPLE IN THE INVERSE COORDINATE REPRESENTATION

A variational principle[1] for obtaining the equilibrium equation (1) is based on the plasma energy

$$W = \int \left(\frac{|B|^2}{2\mu_0} + \frac{p}{\gamma - 1} \right) d^3x \ , \tag{6}$$

where $\gamma \geq 0$ is the adiabatic index. Equation (6) can be shown to be stationary with respect to virtual dispiacements of $\vec{B}$ and p that preserve the magnetic flux and mass density profiles.[1,3] For $\gamma = 0$, W reduces to the Lagrangian (a nondefinite form) introduced by Grad.[2]

The scalar invariance[5] of W can be used to compute it directly in flux coordinates. It is then natural to introduce the inverse representation, for which the real space coordinates $\vec{x}$ are considered to be the <u>dependent</u> variables and the flux coordinates $\vec{a} \equiv (\rho,\theta,\zeta)$ are treated as independent variables during the variation of W. In this representation, the flux and mass conservation constraints must be incorporated into the expressions for $\vec{B}$ and p. Equation (2) already conserves the magnetic flux profiles $\chi'(\rho)$ and $\Phi'(\rho)$. The adiabatic conservation of mass between neighboring flux surfaces requires[1]

$$p(\rho) = M(\rho)\,(V')^{-\gamma} \ , \tag{7}$$

where $V'(\rho) = \int\int d\theta\, d\zeta\, |\sqrt{g}|$ is the differential volume element. Here, the mass function $M(\rho)$ is fixed during the variation of $p(\rho)$ in Eq. (6), whereas $V'(\rho)$, which depends on the geometry of the flux surfaces, may vary. Thus, the energy evaluated in flux coordinates is

$$W = \int \frac{|B|^2}{2\mu_0} |\sqrt{g}|\, d^3\alpha + \int_0^1 \frac{M(\rho)}{\gamma - 1} (V')^{1-\gamma}\, d\rho , \tag{8a}$$

where

$$|B|^2 \equiv B^i B_i = (B^\theta)^2 g_{\theta\theta} + 2B^\theta B^\zeta g_{\theta\zeta} + (B^\zeta)^2 g_{\zeta\zeta} , \tag{8b}$$

$d^3\alpha = d\rho\, d\theta\, d\zeta$, and the outermost flux surface is $\rho = 1$. Summation over repeated Roman indices is implied.

For the toroidal configurations under consideration, a cylindrical coordinate system $\vec{x} = (R,\phi,Z)$ is appropriate, where R is the major radius, ϕ is the toroidal angle, and Z is the height above the midplane (Fig. 1). It then follows that the metric tensor elements are

$$g_{ij} = R_i R_j + R^2 \phi_i \phi_j + Z_i Z_j , \tag{9a}$$

where $R_i = \partial R/\partial\alpha_i$, etc., and $(\alpha_1,\alpha_2,\alpha_3) = (\rho,\theta,\zeta)$. The Jacobian is

$$\sqrt{g} = R \det(G_{ij}) , \tag{9b}$$

$$G_{ij} = \frac{\partial x_i}{\partial \alpha_j} , \tag{9c}$$

where $(x_1,x_2,x_3) = (R,\phi,Z)$. Henceforth, it is assumed that $\sqrt{g} \geq 0$ (i.e.,

there is only a single magnetic axis). Inserting the metric elements into Eq. (8b) yields a cylindrical representation for $|B|^2$,

$$|B|^2 = \frac{b_R^2 + R^2 b_\phi^2 + b_Z^2}{(\sqrt{g})^2}, \tag{10}$$

where $b_i \equiv \sqrt{g}\vec{B} \cdot \nabla x_i = b^\theta (\partial x_i/\partial\theta) + b^\zeta (\partial x_i/\partial\zeta)$ are the cylindrical polar components of $\vec{B}$ and $(b^\theta, b^\zeta) = \sqrt{g}(B^\theta, B^\zeta)$.

To perform the variation of W, suppose that in addition to being functions of the flux coordinates, the cylindrical coordinates $\vec{x}$ and the renormalization parameter λ also depend on an artificial time parameter t. Then, for any scalar function $S(\vec{x},\lambda)$, $\delta S \equiv \partial S/\partial t = (\partial S/\partial x_i)\,\dot{x}_i + (\partial S/\partial\lambda)\,\dot{\lambda}$, and the "time derivative" (i.e., variation) of W in Eq. (8) becomes

$$\frac{dW}{dt} = \int \left[-\left(\frac{|B|^2}{2\mu_0} + p\right)\frac{\partial\sqrt{g}}{\partial t} + \frac{1}{\mu_0\sqrt{g}}\left(b_R\dot{b}_R + R^2 b_\phi\dot{b}_\phi + b_Z\dot{b}_Z + Rb_\phi^2\dot{R}\right)\right] d^3\alpha . \tag{11}$$

Here, $M(\rho)$, $\chi'(\rho)$, and $\Phi'(\rho)$ were held fixed in deriving Eq. (11).

The variation of the polar components of $\vec{B}$ is:

$$\dot{b}_j = b^\theta \frac{\partial\dot{x}_j}{\partial\theta} + b^\zeta \frac{\partial\dot{x}_j}{\partial\zeta} + \dot{b}^\theta \frac{\partial x_j}{\partial\theta} + \dot{b}^\zeta \frac{\partial x_j}{\partial\zeta}, \tag{12a}$$

where $\dot{b}^\alpha(\lambda) = b^\alpha(\dot{\lambda})$. Next, the variation of the Jacobian can be obtained by differentiating Eq. (9b):

$$\frac{\partial\sqrt{g}}{\partial t} = \frac{\dot{R}}{R}\sqrt{g} + \sqrt{g}\left(\frac{\partial \dot{x}_i}{\partial \alpha_j}\frac{\partial \alpha_j}{\partial x_i}\right) , \tag{12b}$$

where $(\sqrt{g}/R)\,\partial\alpha_i/\partial x_j$ is the classical adjoint of G_{ij} (transpose of the cofactors), which is $(\sqrt{g}/R)$ times the inverse of G_{ij}:

$$\frac{\sqrt{g}}{R}\frac{\partial \alpha_i}{\partial x_j} = \begin{bmatrix} \phi_\theta Z_\zeta - \phi_\zeta Z_\theta & R_\zeta Z_\theta - R_\theta Z_\zeta & R_\theta \phi_\zeta - R_\zeta \phi_\theta \\ \phi_\zeta Z_\rho - \phi_\rho Z_\zeta & R_\rho Z_\zeta - R_\zeta Z_\rho & R_\zeta \phi_\rho - R_\rho \phi_\zeta \\ \phi_\rho Z_\theta - \phi_\theta Z_\rho & R_\theta Z_\rho - R_\rho Z_\theta & R_\rho \phi_\theta - R_\theta \phi_\rho \end{bmatrix} . \tag{12c}$$

Using Eq. (12) in Eq. (11) yields

$$\frac{dW}{dt} = -\int F_i \dot{x}_i \, d^3\alpha - \int F_\lambda \dot{\lambda} \, d^3\alpha$$

$$- \int_{\rho=1} |\sqrt{g}| \frac{\partial \rho}{\partial x_i}\left(\frac{|B|^2}{2\mu_0} + p\right)\dot{x}_i \, d\theta \, d\zeta . \tag{13}$$

Here, the MHD force components F_i are

$$F_i = -\frac{\partial}{\partial \alpha_j}\left[|\sqrt{g}|\frac{\partial \alpha_j}{\partial x_i}\left(\frac{|B|^2}{2\mu_0} + p\right)\right] + \mu_0^{-1}|\sqrt{g}|\nabla \cdot \left[(\Lambda_i \vec{B} \cdot \nabla x_i)\vec{B}\right]$$

$$+ \delta_{i1}\frac{|\sqrt{g}|}{R}\left[\frac{|B|^2}{2\mu_0} + p - \frac{R^2(\vec{B}\cdot\nabla\phi)^2}{\mu_0}\right] , \tag{14a}$$

where $\Lambda_1 = \Lambda_3 = 1$, $\Lambda_2 = R^2$ [the index (i) is fixed and not summed in Eq. (14a)], and

$$F_\lambda = \Phi' |\sqrt{g}| F_\beta \quad . \tag{14b}$$

The last term in Eq. (13) is the energy change due to the moving plasma boundary. In Eq. (14), each of the quantities $|B|^2$, $\sqrt{g}$, and $\partial\alpha_j/\partial x_i$ is to be expressed in inverse coordinates as given by Eqs. (8)-(10) and (12c), and $(F_1,F_2,F_3) = (F_R,F_\phi,F_Z)$. Also, $\vec{x}$ is to be considered a function of $\vec{\alpha}$. For example, $\vec{B} \cdot \nabla x_i$ is given explicitly after Eq. (10).

The identity $\nabla \cdot (\vec{e}_i^{cyl}/R) = 0$, which can also be written

$$\frac{\partial}{\partial \alpha_j}\left(\frac{\sqrt{g}}{R}\frac{\partial \alpha_j}{\partial x_i}\right) = 0 \quad , \tag{15}$$

may be used to express F_i in terms of the forces F_ρ and F_β previously defined in Eq. (4) (here $\vec{e}_i^{cyl} \equiv \partial\vec{x}/\partial x_i$):

$$F_i = -|\sqrt{g}|\left[\frac{\partial \rho}{\partial x_i} F_\rho + \left(b^\zeta \frac{\partial \theta}{\partial x_i} - b^\theta \frac{\partial \zeta}{\partial x_i}\right) F_\beta\right] \quad . \tag{16}$$

It follows from Eqs. (4a) and (16) that $-F_i/|\sqrt{g}|$ is the covariant component (in the cylindrical coordinate basis) of the MHD residual force.

For the toroidal systems under consideration here, $\Phi' \neq 0$ (except at $\rho = 0$). It is then possible to choose[4] $\phi = \zeta$. This choice for the magnetic toroidal angle, which is adopted here, simplifies the algebraic structure of Eq. (14), effectively yielding a 2-D Jacobian,

$$\sqrt{g} = RG \quad , \tag{17a}$$

$$G = R_\theta Z_\rho - R_\rho Z_\theta \quad , \tag{17b}$$

and thus reduces the complexity of solving Eq. (14) numerically. In particular, no ζ derivatives appear in $\sqrt{g}$ once ζ is fixed. In addition, the equation $F_\phi = 0$ is redundant, since it follows from Eq. (16) that for $\sqrt{g} \neq 0$, F_ρ and F_β are linear combinations of F_R and F_Z when $\phi = \zeta$. Thus, for a fixed boundary plasma, $\dot{W}$ is stationary when the MHD equilibrium equations $F_\rho = F_\beta = 0$ are satisfied. This proves the energy principle in inverse coordinates for the toroidal angle choice $\phi = \zeta$.

Two-dimensional inverse equilibrium equations $F_i = 0$ were originally derived from a variational principle in Ref. 5 in a form similar to Eq. (16) with $F_\beta = 0$ and were subsequently generalized to three dimensions in Ref. 7. There are, however, several advantages associated with retaining the conservative form of F_i given in Eq. (14). Since F_i is a second-order differential operator in flux coordinates, a conservative finite-difference representation for F_i (in ρ) is readily derived by integrating Eq. (14) on a radial mesh. Spectral analysis of F_i is facilitated by integrating Eq. (14) by parts in θ and ζ (see Sec. VIII). In this way, no derivatives of R, Z, or λ higher than first order are required for the numerical evaluation of F_i. Finally, the boundary condition at a free boundary ($\rho = 1$), which requires the continuity of the total pressure, is easily implemented when F_i is in a conservative form.

In contrast to the axisymmetric case, where $F_\lambda = 0$ may be analytically integrated [cf. Eq. (5a)], in three dimensions it is necessary to solve this equation numerically. From Eq. (4e), it is apparent that the relation $F_\lambda = 0$ is a <u>linear</u> elliptic equation for λ on each flux surface. As noted previously, by introducing λ in Eq. (2), the number of Fourier harmonics required for an accurate inverse representation of $\mathbf{x}(\rho,\theta,\zeta)$ is reduced. Since the Fourier coefficients of $\mathbf{x}$ satisfy moments of the <u>nonlinear</u>

equations $F_i = 0$ (see Sec. IV), the introduction of λ actually simplifies the solution of the equilibrium problem by accelerating the convergence of the Fourier series for $\mathcal{R}$, even though additional linear equations must be solved.

With the magnetic toroidal angle ζ chosen equal to the geometric toroidal angle ϕ, the conservative expressions for the two force components F_R and F_Z become particularly simple:

$$F_R = \frac{\partial}{\partial\rho}(Z_\theta P) - \frac{\partial}{\partial\theta}(Z_\rho P) + \mu_0^{-1}\left[\frac{\partial}{\partial\theta}(B^\theta b_R) + \frac{\partial}{\partial\zeta}(B^\zeta b_R)\right] + G\left[\frac{P}{R} - \frac{(RB^\zeta)^2}{\mu_0}\right], \tag{18a}$$

$$F_Z = -\frac{\partial}{\partial\rho}(R_\theta P) + \frac{\partial}{\partial\theta}(R_\rho P) + \mu_0^{-1}\left[\frac{\partial}{\partial\theta}(B^\theta b_Z) + \frac{\partial}{\partial\zeta}(B^\zeta b_Z)\right], \tag{18b}$$

where $P = R(p + |B|^2/2\mu_0)$ and b_i is defined after Eq. (10). This result can also be derived by taking components of the MHD residual force (see Appendix A). The significance of the present variational derivation will become evident in the following sections.

Note from Eqs. (14b) and (16) that when the angle renormalization parameter λ is retained, the equations for R, Z, and λ are dependent, since there are only two independent MHD forces F_ρ and F_β. This underdetermination is resolved by specifying the poloidal angle variable θ. The choice of θ adopted here, which is dictated by the economization of the finite Fourier expansions for R and Z and is different from previous angle specifications,[4,5,7] is described in Appendix B.

IV. STEEPEST DESCENT METHOD OF SOLUTION FOR THE MOMENT EQUATIONS

The inverse mapping $\mathcal{X} = \mathcal{X}(\rho,\theta,\zeta)$ can be expressed as an explicit function of the flux coordinates as follows:

$$R = R_0(\rho) + p_R(\rho,\theta,\zeta) \ , \tag{19a}$$

$$Z = Z_0(\rho) + p_Z(\rho,\theta,\zeta) \ . \tag{19b}$$

Here, p_j (for $j = 1,3$) are periodic functions of the angles, that is, $\iint d\theta\, d\zeta\, p_j = 0$. The moment representation of the equilibrium results from expanding p_j and λ in Fourier series. Defining $(x_1,x_2,x_3) \equiv (R,\lambda,Z)$, where λ now replaces the fixed toroidal angle $\zeta = \phi$ as a coordinate, and the associated complex Fourier amplitudes X_j^{mn}, Eq. (19) becomes

$$x_j = \sum_{m,n} X_j^{mn}(\rho)\exp[i(m\theta - n\zeta)] \ . \tag{20}$$

The reality of x_j implies $X_j^{mn} = (X_j^{-m,-n})^*$. Since λ is periodic, $X_2^{00} = 0$.

Using the representation of x_j given in Eq. (20), the variation of the energy in Eq. (13) becomes (neglecting the surface terms)

$$\frac{dW}{dt} = -\int (F_j^{mn})^* \frac{\partial X_j^{mn}}{\partial t}\, dV \ , \tag{21a}$$

where

$$F_j^{mn} = (V')^{-1} \iint F_j \exp[-i(m\theta - n\zeta)]\, d\theta\, d\zeta \ , \tag{21b}$$

$F_1 = F_R$, $F_2 = F_\lambda$, $F_3 = F_Z$, and $dV = V'\, d\rho$. The volume factor $V' = \partial V/\partial\rho$ normalizes the force coefficients to ensure the correct asymptotic

dependence on ρ at the magnetic axis ($\rho = 0$) and in practice is chosen to be the differential volume V_j' corresponding to the initial plasma state.

The Fourier coefficients $F_j^{mn} = (F_j^{-m,-n})^*$ are the variational forces that must vanish in equilibrium.[5,7] By considering the moment amplitudes X_j^{mn} as independent trial functions in a Ritz method (subject to the reality constraint), it is seen that the equations $F_j^{mn} = 0$ represent the most accurate system for determining the X_j^{mn} that result from a finite truncation of the series in Eq. (20). Previously, this system of nonlinear, second-order, ordinary differential equations has been solved in two dimensions by direct Jacobian inversion methods.[5,7] In three dimensions, the larger number of moment amplitudes needed to describe an equilibrium can significantly decrease the efficiency and numerical stability of such direct methods. Therefore, an iteration method is now developed for following the path, in the phase space of the moment amplitudes, along which $\dot{W}$ decreases at a maximum rate.

Since W is bounded from below due to flux and mass ($\rho^{1/\gamma}$) conservation and is positive definite for $\gamma > 1$, the equilibrium corresponds to a minimum energy state.[1] Thus, by finding the path along which $\dot{W}$ decreases monotonically, an equilibrium will eventually be reached. To minimize $\dot{W}$ in Eq. (21a), note that $\left|\int F_j^* \dot{x}_j \, dV\right|^2 \le \int \sum_j |F_j|^2 \, dV \int \sum_j |\dot{x}_j|^2 \, dV$, with equality pertaining if and only if $\dot{x}_j = kF_j$, where k is an arbitrary real constant (k = 1 here). Thus, the descent path is

$$\frac{\partial X_j^{mn}}{\partial t} = F_j^{mn} \quad , \tag{22a}$$

and the maximum rate of decrease in W along this path is given by

$$\frac{dW}{dt} = -\sum_{j,m,n} \int |F_j^{mn}|^2 \, dV \, . \tag{22b}$$

Equation (22) comprises the descent equations for relaxing W to its minimum energy state. It is the Fourier space analogue of the descent equations derived in Ref. 4. Note that $\dot{W} = 0$ if and only if $F_j^{mn} = 0$ for all j, m, and n (that is, when all the equilibrium equations are satisfied simultaneously).

Since F_j^{mn} correspond to second-order differential operators in ρ, the descent equation (22a) comprises a set of parabolic differential equations. The convergence to an equilibrium solution is prohibitively slow[10,11] for an explicitly differenced version of Eq. (22a). Implicit schemes,[11] which remove the small time step required for stability of explicit schemes, are impractical here since the forces F_j^{mn} are strongly nonlinear functions of the amplitudes X_j^{mn}. The convergence of these equations can be accelerated, while retaining an explicit form for the forces, by converting them to hyperbolic equations[10] (the second-order Richardson scheme):

$$\frac{\partial^2 X_j^{mn}}{\partial t^2} + \frac{1}{\tau}\frac{\partial X_j^{mn}}{\partial t} = F_j^{mn} \, . \tag{23}$$

The parameter $\tau > 0$ has little effect on the stability of the numerical scheme[10] and can therefore be chosen to maximize the decay rate of the least damped mode of Eq. (23), thereby minimizing the number of iterations required to reach steady state. The optimum value for τ, leading to critical damping in Eq. (23), is[10]

$$\frac{1}{\tau_{op}} \simeq -\frac{d}{dt}\left(\ln \int |F|^2 \, dV\right) \quad , \tag{24}$$

where $\int |F|^2 \, dV \equiv \int \sum_{j,m,n} |F_j^{mn}|^2 \, dV$. There is an energy principle associated with the second-order system equation (23). Multiplying Eq. (23) by $V_i^j(\dot{X}_j^{mn})^*$, taking complex conjugates, and using Eq. (21a) for $\dot{W}$ yields

$$\frac{d}{dt}(W_K + W) = -\frac{2}{\tau} W_K \quad , \tag{25}$$

where $W_K = \int |\dot{X}|^2/2 \, dV$ is the kinetic energy. Thus, for $\tau > 0$, the sum of the kinetic and potential energies, which is bounded from below, decays monotonically until $W_K = 0$ and equilibrium is attained.

V. BOUNDARY AND INITIAL CONDITIONS

The magnetic axis ($\rho = 0$) is a singular curve of the coordinate system where $\nabla\chi = 0$. For toroidally nested surfaces, this corresponds to the one parameter space curve $R = R_0(\zeta)$, $Z = Z_0(\zeta)$. The geometry of the magnetic axis is determined by Taylor expanding χ in $x = R - R_0$ and $y = Z - Z_0$:

$$\chi = \alpha(\zeta)x^2 + 2\beta(\zeta)xy + \gamma(\zeta)y^2 + \ldots \quad , \tag{26}$$

where $\alpha\gamma - \beta^2 > 0$ for elliptical surfaces encircling the magnetic axis. In terms of the moment amplitudes this implies (for $j = 1,3$):

$$X_j^{mn}(\rho = 0, t) = 0 \; ; \quad m \neq 0 \quad . \tag{27a}$$

In fact, if $V(\rho) = \int_0^\rho V' \, d\rho$ is the volume inside a flux surface, then $X_j^{mn} \sim V^{m/2}$ as $\rho \to 0$. Since the magnetic axis corresponds to an extremum of the flux (or pressure) contours, the radial variation of $[R_0(\zeta), Z_0(\zeta)]$ must be second order near $\rho = 0$. Hence, for $j = 1,3$:

$$\frac{dX_j^{0n}}{d\rho}(\rho = 0,t) \sim \lim_{\rho \to 0} V'(\rho) \ . \tag{27b}$$

For the typical case when $\rho \sim \sqrt{V}$, Eq. (27b) reduces to $(X_j^{0n})' = 0$. For $j = 2 (x_2 = \lambda)$, the origin boundary condition may be deduced by noting from Eq. (4e), together with the fact that R_θ and Z_θ both vanish at the magnetic axis, that

$$\lim_{V \to 0} \lambda_\theta = \frac{\sqrt{g}}{\oint \sqrt{g} \, d\theta} - 1 \ . \tag{27c}$$

Equations (27a) and (27b) imply $R = R_0(\zeta) + \rho[r_1(\zeta)\cos\theta + r_2(\zeta)\sin\theta] + O(\rho^2)$, with a similar expansion for Z, and hence $\sqrt{g} = V'[g_0(\zeta) + V^{1/2} g_1(\theta,\zeta)]$. Since $g_0(\zeta)$ is independent of θ, Eq. (27c) yields $\partial X_2^{mn}(\rho = 0,t)/\partial\theta = 0$. This boundary condition given here differs from those in Ref. 4, due to the polar representation used there.

Now consider two types of boundary conditions that may be imposed at the plasma edge.

A. Fixed boundary

In this case, the shape of the outermost flux surface ($\rho = 1$) is fixed for all times. When the poloidal angle renormalization parameter λ is

retained, this is equivalent to prescribing the individual Fourier harmonics of both R and Z at $\rho = 1$ (see Appendix B):

$$X_j^{mn}(\rho = 1,t) = X_j^{mn}_b \qquad (28)$$

for $j = 1,3$. No boundary condition is needed for $x_2 = \lambda$, since F_λ is local in ρ (there are no radial derivatives of λ in F_λ). In this representation, the angle coordinate λ accounts for the rotation of the magnetic field lines in the poloidal direction during the minimization of W.

B. Free boundary

The position of the free plasma boundary is determined by the continuity of the total pressure $|B|^2/2\mu_0 + p$ at the plasma-vacuum interface ($\rho = 1$) and by the vanishing of the normal component of the vacuum field over this surface. These boundary conditions can be incorporated into the variational principle[1,4] by appending the vacuum magnetic energy to the plasma energy W_{pl} given in Eq. (8). The total energy functional then becomes:

$$W = W_{pl} - W_v = \int_{plasma} \left(\frac{|B|^2}{2\mu_0} + p\right) d^3x - \int_{vacuum} \frac{|\nabla v|^2}{2\mu_0} d^3x \,, \qquad (29)$$

where $\vec{B}_v = -\nabla v$ is the vacuum magnetic field. (This representation for $\vec{B}_v$ conserves the total plasma and vacuum coil currents.) The minus sign in Eq. (29) guarantees the continuity of the total pressure at the plasma-vacuum interface. In the plasma, where the magnetic flux is conserved on each flux surface, a change in the position of the boundary produces a reciprocal variation in the energy. [Thus, there is a minus

sign in the last term of Eq. (13).] In general, the vacuum region will contain current-carrying coils surrounded by a conducting wall. The vacuum integral in Eq. (29) must then be separated into regions bounded by the coil surfaces, with appropriate jumps in ν to account for the coil currents.

Taking the time derivative of Eq. (29) and using Eq. (13) to evaluate the plasma energy change yields

$$\frac{dW}{dt} = -\int F_i \dot{x}_i \, d^3\alpha + \mu_0^{-1} \int_{\text{vacuum}} \dot{\nu} F_\nu \, d^3x - \int_{\rho=1} S_i \dot{x}_i \, d\theta \, d\zeta$$
$$- \mu_0^{-1} \left(\int_{\rho=1} \dot{\nu} \vec{B}_\nu \cdot d\vec{S}_\rho - \int_{\text{wall}} \dot{\nu} \vec{B}_\nu \cdot d\vec{S} \right) , \tag{30}$$

where

$$S_i = \left[|\sqrt{g}| \frac{\partial \rho}{\partial x_i} \left(\frac{|B|^2}{2\mu_0} + p - \frac{|\nabla \nu|^2}{2\mu_0} \right) \right]_{\rho=1} \tag{31a}$$

is the pressure jump at the plasma-vacuum interface, $|B|^2$ is the magnetic field strength in the plasma given by Eq. (8b), $d\vec{S}_\rho = \nabla\rho |\sqrt{g}| \, d\theta \, d\zeta$, and

$$F_\nu \equiv -\nabla \cdot \vec{B}_\nu = \nabla^2 \nu \tag{31b}$$

is the vacuum "force." The last term in S_i represents the vacuum energy change due to the motion of the free boundary. Thus, the descent equation for the vacuum potential is

$$\dot{\nu} = F_\nu \, . \tag{31c}$$

Equation (30) is a minimax principle for the plasma-vacuum equilibrium configuration. The physical boundary conditions, which require

$\vec{B}_v \cdot d\vec{S}_\rho = 0$ and $S_i = 0$ at $\rho = 1$ and $\vec{B}_v \cdot d\vec{S} = 0$ at the conducting wall, are also natural boundary conditions for the extremization of W. The solution of Eq. (31c) using a Fourier series expansion for ν is discussed in Appendix C.

Now, consider the initial conditions needed to integrate Eq. (23). Both X_j^{mn} and $\dot{X}_j^{mn}$ must be prescribed at the beginning of the descent. To guarantee that W will decrease at $t = 0$, it is convenient to take

$$\dot{X}_j^{mn} = \alpha F_j^{mn} \quad . \tag{32a}$$

In practice, $\alpha \simeq 0$ provides a sufficiently well-behaved start for the descent equations. The initial profiles $X_j^{mn}(\rho)$ are chosen consistent with the boundary conditions at $\rho = 0$ and $\rho = 1$. From Eqs. (27) and (28), it follows that for $j \neq 2$:

$$X_j^{mn}(\rho,0) = \begin{cases} v(\rho) X_{jb}^{mn} & m \neq 0 \\ X_{jb}^{0n} & m = 0 \quad , \end{cases} \tag{32b}$$

where X_{jb}^{mn} are the initial boundary data. For $j = 2$, $\lambda^{mn} = X_2^{mn}(\rho, 0) = 0$ is used in practice.

In Eq. (32b), $v(\rho)$ is a monotonic function of ρ satisfying $v(1) = 1$ and $v(0) = 0$. [A small boundary layer near the magnetic axis where $X_j^{mn} \sim \rho^{m/2}$ is neglected by the ansatz in Eq. (32b).] Geometrically, $v(\rho)$ is simply related to the initial plasma volume in an equivalent infinite-aspect-ratio system ($R \to \infty$):

$$v(\rho) = \left[\frac{V_\infty(\rho, 0)}{V_\infty(1, 0)}\right]^{1/2} , \tag{32c}$$

where $V_\infty = R_m \int G \, d\theta \, d\zeta$. Here, G is the 2-D Jacobian defined in Eq. (17b), and R_m is the mean radius of the magnetic axis. The radial grid can be adjusted by choosing the functional form for $v(\rho)$. For example, $v(\rho) = \rho$ identifies ρ with the the usual polar radius, whereas $v(\rho) = \rho^{1/2}$ makes ρ a measure of the volume inside a flux surface.[4]

There are other possible ways of choosing ρ. For tokamaks and stellarators with strong uniform toroidal magnetic fields, $\Phi(\rho)$ is monotonic and a magnetic prescription

$$\rho = \left[\frac{\Phi(\rho)}{\Phi(1)}\right]^{1/2} \tag{32d}$$

can be used. In Refs. 5 and 7, $-\rho$ was chosen to be the cos θ harmonic of R. The poloidal flux $\chi'(\rho)$ was then determined from the surface-averaged force balance equation, $\langle \sqrt{g} F_\rho \rangle \equiv \iint \sqrt{g} F_\rho \, d\theta \, d\zeta = 0$, which results from varying the energy with respect to χ at fixed $\iota(\chi)$ and $p(\chi)$. This equation is not, however, independent of the other moment equations $F_j^{mn} = 0$. Indeed, Eq. (16) can be used to show that

$$\langle \sqrt{g} F_\rho \rangle = - \sum_{m,n} \left[(X_R^{mn})' (F_R^{mn})^* + (X_Z^{mn})' (F_Z^{mn})^* \right] .$$

Thus, the various prescriptions for ρ are related, but only those given by Eqs. (32c,d) preserve the symmetry of the descent equations.

Once the radial coordinate is specified, the initial magnetic and pressure profiles can be chosen so that the surface-averaged pressure

balance equation $\langle\sqrt{g}F_\rho\rangle = 0$ will be satisfied at $t = 0$. (In the 2-D problem considered in Ref. 5, the average pressure balance was satisfied at all times by changing from magnetic flux to current flux variables. This procedure does not, however, generalize to three dimensions.) For example, for fixed ι and p profiles, the toroidal flux Φ may be rescaled with respect to ρ so that the average pressure balance

$$\langle(\sqrt{g}\vec{J}\cdot\nabla\zeta)(\sqrt{g}\vec{B}\cdot\nabla\theta)\rangle - \langle(\sqrt{g}\vec{J}\cdot\nabla\theta)(\sqrt{g}\vec{B}\cdot\nabla\zeta)\rangle + \mu_0 p'V' = 0 \ , \quad (33a)$$

where $\langle A\rangle = \iint d\theta\, d\zeta\, A$ and $V' = \langle\sqrt{g}\rangle$, is satisfied. This generally improves the convergence rate of the descent algorithm. Using the explicit forms for B^θ and B^ζ given in Eq. (3), integrating the λ_θ and λ_ζ derivative terms by parts, and assuming $F_\beta \simeq 0$, Eq. (33a) becomes:

$$\chi' J'_\zeta - \Phi' J'_\theta + \mu_0 p' V' = 0 \ , \quad (33b)$$

where $J'_\theta \equiv \langle\sqrt{g}\vec{J}\cdot\nabla\theta\rangle = -\partial\langle B_\zeta\rangle/\partial\rho$ and $J'_\zeta \equiv \langle\sqrt{g}\vec{J}\cdot\nabla\zeta\rangle = \partial\langle B_\theta\rangle/\partial\rho$ are the current fluxes. Equation (33b) is exact when $F_\beta = 0$ or $\lambda = 0$. Assuming that the pressure and rotational transform profiles are prescribed functions of the initial volume $v(\rho)$, so that $\chi' = \iota(v)\Phi'$ and $p' = (\partial p/\partial v)(\partial v/\partial\rho)$, Eq. (33b) becomes a linear first-order differential equation for $h(\rho)$, where $\Phi'(\rho) = (\partial v/\partial\rho)\,[2h(\rho)]^{1/2}$ and h is regular at $\rho = 0$,

$$\frac{\partial}{\partial\rho}\left[(\iota^2\hat{g}_{\theta\theta} + 2\iota\hat{g}_{\theta\zeta} + \hat{g}_{\zeta\zeta})h\right] + (\iota^2\hat{g}'_{\theta\theta} + 2\iota\hat{g}'_{\theta\zeta} + \hat{g}'_{\zeta\zeta})h + \mu_0 p_v V' = 0 \ . \quad (34)$$

Here, $\hat{g}_{ij} \equiv (\partial v/\partial \rho) \langle g_{ij}/\sqrt{g} \rangle$, $p_v = \partial p/\partial v$, and $\sqrt{g} = R\,(\partial v^2/\partial \rho)\, G(\theta,\zeta)$.

Equation (33b) provides a practical numerical criterion for the convergence to an equilibrium. Forming the quantity

$$Q \equiv \frac{\chi' J_\zeta' - \Phi' J_\theta' + \mu_0 p' V'}{|\chi' J_\zeta'| + |\Phi' J_\theta'| + \mu_0 |p'| V'} , \tag{35}$$

note that a converged equilibrium is attained when Q is less than the spatial discretization error.

VI. GEOMETRIC CONSTRAINTS ON THE FORM OF THE INVERSE REPRESENTATION

The terms of the Fourier series comprising the moment expansions of R and Z in Eq. (20) are determined both by the shape of the magnetic flux surfaces and by the symmetry, or periodicity, of the plasma confinement geometry. In two dimensions, it is well known[9] that the first few terms in the moment expansion can be related to certain specific geometric properties of the flux surfaces such as the major axis Shafranov shift, ellipticity, triangularity, bean-shapedness, etc. In addition, since R and Z are individually Fourier expanded, it is possible to represent "non-starlike" domains for which $r^2 = \bar{R}^2 + \bar{Z}^2$ is not a single-valued function of the real poloidal angle $\theta' = \tan^{-1}\bar{Z}/\bar{R}$. [Here, $\bar{R} = R - R_0$, $\bar{Z} = Z - Z_0$ are coordinates centered at the position of the magnetic axis (R_0, Z_0).]

To extend these concepts to three dimensions, consider the possible transformations of a flux surface as it rotates in the toroidal direction.

Specifically, consider the near-axis expansion of a helically invariant equilibrium:

$$r^2 - b_\ell r^\ell \cos(\ell\theta - N\phi) = (r_0)^2 \ , \tag{36a}$$

where $b_\ell << 1$ is related to the helical current strength, N is the toroidal field period, and $\theta = \theta'$. To first order in b_ℓ, Eq. (36a) can be written:

$$r^2 = (r_0)^2 + \hat{b}_\ell \cos(\ell\theta - N\phi) \ . \tag{36b}$$

Thus, for $\hat{b}_\ell = 0$, the surfaces are circles, which have the moment expansion $\bar{R} = -r_0 \cos\theta$, $\bar{Z} = r_0 \sin\theta$. Since θ only enters this moment representation as a parameter, it can, in principle, be replaced by <u>any</u> function $\hat{\theta}(\theta,\phi)$ without affecting the surface shape. However, $\hat{\theta}$ is determined uniquely (up to an arbitrary periodic function of θ) by periodicity and symmetry constraints. First, since $r = r_0$ is obviously axisymmetry, $\partial\hat{\theta}/\partial\phi = 0$. Second, since $\bar{R}$ (and $\bar{Z}$) must be periodic with period 2π, $\hat{\theta} = \theta + p(\theta)$ results. (This precludes stretching transformations of the form $\hat{\theta} = k\theta$ for integers $|k| > 1$.)

Now, consider the transformations of the magnetic surfaces embodied in Eq. (36b) when $\hat{b}_\ell \neq 0$.

A. Toroidal ripple

This case ($\ell = 0$) corresponds to a circular cross-section tokamak with N finite toroidal field coils. The flux surfaces in the axisymmetric limit are now modulated in minor radius at the spatial wave number $\phi_N = N\phi$:

$$\bar{R} = -r_0 \cos\theta(1 + \alpha_0 \cos\phi_N) \ , \tag{37a}$$

$$\bar{Z} = r_0 \sin\theta(1 + \alpha_0 \cos\phi_N) \ , \tag{37b}$$

where $\alpha_0 = \hat{b}_0/2(r_0)^2$. The modulation of more complex cross-sectional shapes can be modeled by multiplicative factors depending on ϕ_N as in Eq. (3[illegible] at, in addition to cos θ (or sin θ) terms, the Fourier series for $\bar{R}$ [illegible] now contains $\cos(\theta \pm \phi_N)$ [or $\sin(\theta \pm \phi_N)$] terms as well.

B. Helical magnetic axis

For $\ell = 1$, there is a shift of the magnetic axis that varies periodically in the toroidal direction:

$$\bar{R} = -\alpha_1 \cos\phi_N - r_0 \cos\theta \tag{38a}$$

$$\bar{Z} = \alpha_1 \sin\phi_N + r_0 \sin\theta \ , \tag{38b}$$

where $\alpha_1 = \hat{b}_1/2r_0$ is the helical shift. Note that even though $\bar{R}$ and $\bar{Z}$ are not helically invariant functions by themselves, they do combine to form flux surfaces r_0 = const that depend only on the angle combination $\ell\theta - N\phi$.

C. Rotating elliptical cross section

When $\ell = 2$, Eq. (38b) represents an ellipse with elongation $\kappa = (1 - \alpha_2)/(1 + \alpha_2)$, where $\alpha_2 = b_2/2r_0$:

$$\bar{R} = -r_0 \cos\theta - \alpha_2 \cos(\theta - \phi_N) \ , \tag{39a}$$

$$\bar{Z} = r_0 \sin\theta - \alpha_2 \sin(\theta - \theta_N) \quad . \tag{39b}$$

In three dimensions, the helically invariant rotations considered so far must be generalized to account for effects due to (i) changes in the flux surface shape as the toroidal angle is traversed or (ii) a differential rotation rate (with ϕ_N) for the various poloidal harmonics composing R and Z. As an example of the former effect, which is characteristic of helically wound toroidal systems where some poloidal harmonic mixing invariably occurs due to the dependence of the major radius R on θ, a flux surface may deform continuously from an elliptical cross section into a triangular, D-shaped one as ϕ_N increases. Both effects can be incorporated into the moment representation by taking $0 \leq m \leq M$ and $-N \leq n \leq N$, where $M \lesssim 3$ is sufficient to describe a wide variety of cross-section shapes and $N \lesssim 2$ can account for many effects of nonuniform toroidal rotation and changing cross-section shapes.

VII. MOMENT ANALYSIS OF SOLOV'EV EQUILIBRIUM

An exact analytic solution of a 2-D equilibrium problem[12] in the inverse coordinate representation will now be considered. This will emphasize the importance of distinguishing between the geometric angle θ appearing in the Fourier representation of the flux surfaces and the magnetic angle $\theta^* = \theta + \lambda$ [Eq. (3a)], which describes straight magnetic field lines. A solution of the axisymmetric Grad-Shafranov equation[12] when the magnetic field is represented as $\vec{B} = \chi' \nabla\zeta \times \nabla\rho + F(\rho)\nabla\zeta$ is

$$\rho^2 = \frac{\beta_1}{\chi_0^2}\left[Z^2R_0^2 + \left(\frac{\beta_0}{8\beta_1}\right)(R^2 - R_m^2)^2\right] , \tag{40}$$

where $\chi' = 2\rho\chi_0$ (ρ is the normalized poloidal flux, $0 \le \rho \le 1$), $p(\rho) = \beta_0(1 - \rho^2)$, and $F^2 = R_0^2(1 - 4\beta_1\rho^2)$. The toroidal field is normalized to unity if R_0 is identified with the mean major radius. Note that $R = R_m$ is the magnetic axis, which is determined by the boundary curve $\rho = 1$. The spectral analysis of Eq. (40) is trivial in terms of the variables $u = R^2$ and Z, yielding

$$u = R_m^2 - \chi_0(8/\beta_0)^{1/2}\rho \cos\theta , \tag{41a}$$

$$Z = (\chi_0/R_0)\beta_1^{-1/2}\rho \sin\theta . \tag{41b}$$

Here, θ is a geometric angle yielding a rapidly convergent Fourier expansion for R and Z, which is not equal to the magnetic angle θ^* in which field lines are straight. To show this, note that the Jacobian is

$$\sqrt{g} = \frac{\chi_0^2}{R_0}\left(\frac{2}{\beta_0\beta_1}\right)^{1/2}\rho . \tag{42}$$

Thus, $\sqrt{g}/R^2$ is not a function of ρ alone, as Eq. (5c) requires for $\lambda = 0$. Therefore, even though the geometric solution given in Eq. (41) satisfies the equilibrium Grad-Shafranov equation, it apparently fails to simultaneously satisfy $J^\rho = F_\beta = 0$ when $\lambda = 0$. By introducing the angle renormalization parameter λ, the angle θ can be chosen for its geometric properties while the constraint $F_\beta = 0$ is satisfied by λ. For the present example, it is easy to evaluate λ explicitly from Eq. (5c):

$$\lambda_\theta = \frac{(1 - a^2)^{1/2}}{1 - a \cos\theta} - 1 , \tag{43a}$$

where $a(\rho) = \chi_0(8/\beta_0)^{1/2}\rho/R_m^2 < 1$. Thus, $\lambda = \sum_{m=1} \lambda_m \sin m\theta$, where

$$\lambda_m = \frac{2}{m}\left[\frac{1 - (1 - a^2)^{1/2}}{a}\right]^m . \tag{43b}$$

Note that for $a^2 < 1$, λ_m decays exponentially with m. Similarly, the magnetic flux profile is found to be:

$$\frac{\Phi'}{\chi'} \equiv q(\rho) = \frac{\chi_0}{R_m^2}\left[\frac{1}{2\beta_0\beta_1}\left(\frac{1 - 4\beta_1\rho^2}{1 - a^2}\right)\right]^{1/2} . \tag{44}$$

The results in Eqs. (42)-(44) provide an analytic basis for testing the computational methods developed here (see Sec. X). They also reveal the fundamental incompatibility, in the absence of angle renormalization, between an economical Fourier description of the flux surface geometry and the MHD constraint, $J^\rho = 0$.

VIII. NUMERICAL METHOD

In this section, some numerical aspects of solving the descent equations are considered. First, the time discretization of Eq. (23) is discussed, and an estimate for the maximum stable time step is obtained. Then, the spatial discretization of the forces F_j^{mn} is performed, including the incorporation of the boundary conditions considered in Sec. V.

A. Time discretization

The descent equations (23) for the plasma can be written

$$\frac{d}{dt} S(t)\dot{X}_j^{mn} = S(t)F_j^{mn} , \tag{45}$$

where $S(t) = \exp \int^t \tau^{-1}\, dt'$. Integrating Eq. (45) from $t = t_{n-1/2}$ to $t = t_{n+1/2}$, where t_n is the time at the nth iteration, yields

$$\dot{X}_j^{mn}(t_{n+1/2}) = (1 - b_n)\dot{X}_j^{mn}(t_{n-1/2}) + \left(1 - \tfrac{1}{2}b_n\right)\Delta t F_j^{mn}(t_n) , \tag{46a}$$

where $\Delta t = t_{n+1/2} - t_{n-1/2}$,

$$\dot{X}_j^{mn}(t_{n+1/2}) = \frac{X_j^{mn}(t_{n+1}) - X_j^{mn}(t_n)}{\Delta t} + O(\Delta t^2) \tag{46b}$$

is the discretized "velocity," and

$$b_n = 1 - \exp\left(- \int_{t_{n-1/2}}^{t_{n+1/2}} \frac{1}{\tau}\, dt\right) \tag{46c}$$

is the incremental damping factor. Using the expression for $1/\tau$ given in Eq. (24) and adding a small minimum damping rate $(\tau^{-1})_{min}$ (to guarantee convergence near the energy minimum[3]) yields

$$b_n = 1 - y_n(1 - b_{min}) , \tag{46d}$$

where $y_n = \min(\langle F^2\rangle_n/\langle F^2\rangle_{n-1},\ \langle F^2\rangle_{n-1}/\langle F^2\rangle_n)$, $b_{min} = (\tau^{-1})_{min}\Delta t$, and $\langle F^2\rangle_n = \int |F(t_n)|^2\, dV$. With this form for b_n, Eq. (46a) reduces to the "conjugate gradient" procedure used in Ref. 3. In practice, since b_n is

proportional to the algebraically largest eigenvalue of $\vec{\vec{F}}$, y_n should be averaged[4] over several iterations to reduce the effect of a mixture of eigenvectors. Since the longest damping time scales as $N_\rho \Delta t$, where N_ρ is the number of radial mesh points, an average over N_ρ previous iterations is approximately equivalent to averaging over one e-folding decay time.

The maximum stable time step Δt may be estimated from a von Neumann analysis[11] of the linearized version of Eq. (46a). The result is:

$$\Delta t_{max} = \left(\frac{4}{|\lambda_{max}|} \right)^{1/2} , \tag{47}$$

where $|\lambda_{max}|$ is the modulus of the algebraically smallest eigenvalue of $\vec{\vec{F}}$. Equation (47) is $(|\lambda_{max}|)^{1/2} >> 1$ times larger than the stable time step for an equivalent first-order time scheme.

To estimate λ_{max}, consider the eigenvalues of the spatially discretized and linearized operator $\vec{\vec{F}}$. Noting that the shortest radial wavelengths in the F_R and F_Z operators will determine λ_{max}, we can approximate the eigenvalue condition using only the highest-order ρ derivatives in Eq. (18). Denoting the kth eigenvector by (R_k, Z_k), Eq. (18) reduces in the short-wavelength limit to

$$D_{RR} R_k'' - D_{RZ} Z_k'' = -\lambda_k R_k , \tag{48a}$$

$$-D_{RZ} R_k'' + D_{ZZ} Z_k'' = -\lambda_k Z_k , \tag{48b}$$

where $D_{RR} = Z_\theta^2 d_0$, $D_{RZ} = Z_\theta R_\theta d_0$, $D_{ZZ} = R_\theta^2 d_0$, $d_0 = R|B|^2/(GV_i'\mu_0)$, and $G = \sqrt{g}/R$. For short-wavelength modes, the diffusion coefficients in Eq. (48) can be treated as constants (in a WKB sense). The spatial discretization for the second-order derivatives in Eq. (48) is taken to be:

$$R''(\rho = \rho_n) \simeq \frac{R(\rho_{n+1}) - 2R(\rho_n) + R(\rho_{n-1})}{(\Delta\rho)^2}, \tag{49}$$

and similarly for Z'', where $\Delta\rho = \rho_n - \rho_{n-1}$ is the uniform radial grid spacing. Letting $R_k(n) = R_0 \exp(in\beta_0)$, where β_0 is a real phase factor, it is apparent that $R_k''(n) = -4R_k(n)\sin^2(\beta_0/2)/(\Delta\rho)^2$. Using this result and applying Gerschgorin's theorem[11] to account for a nonuniform ρ dependence of the diffusion coefficients, it follows from Eq. (48) that

$$\begin{aligned} \max_k |\lambda_k| &\leq \frac{4}{(\Delta\rho)^2} \max_{\rho,\theta,\zeta} \left\{ \left[\max(D_{RR}, D_{ZZ}) \right]^{1/2} \left[D_{RR}^{1/2} + D_{ZZ}^{1/2} \right] \right\} \\ &\simeq \frac{4 g_{\theta\theta}}{(\Delta\rho)^2} \left(\frac{|B|^2}{2\mu_0} \right), \end{aligned} \tag{50}$$

where $g_{\theta\theta} = 2Rg_{\theta\theta}/(GV_i')$. Obviously, λ_k^{-1} is related to the time for an Alfvén wave to travel across the radial mesh. Note that $\Delta\rho = (N_\rho - 1)^{-1}$, which implies $\max|\lambda_k| \sim N_\rho^2$. When the cylindrical nature of the eigenfunctions of Eq. (48) is accounted for, it is found that $\Delta\rho$ in Eq. (50) is replaced by $(N_\rho + M/2 - 1)^{-1}$, where M is the maximum poloidal mode number.

It is now possible to make a heuristic comparison between the steepest descent method and the Jacobian inversion methods used previously[5,7] to solve the equilibrium moment equations. The Jacobian methods involve inverting the linearized $\vec{F}$ operator and hence determining <u>all</u> the eigenvalues of this operator. In contrast, the steepest descent method requires only an estimate for the <u>largest</u> eigenvalue of $\vec{F}$. When the number of eigenvalues is large (i.e., for a stiff system), an accurate inversion

of $\vec{F}$ becomes prohibitively time-consuming, and the accelerated descent method seems preferable.

B. Spatial discretization of the forces

The continuous expressions for the MHD residual forces obtained in Secs. III and IV may be transformed into discrete forms by numerical integration of W.[13] Discrete conservative forms for the Fourier-transformed forces are then obtained by varying the individual nodal amplitudes.[4] The asymptotic behavior of the solutions near the magnetic axis is used to appropriately modify these nodal equations in the vicinity of $\rho = 0$.

The angle integrals in Eq. (8) are replaced by discrete sums as follows:[13]

$$W \equiv \int d\rho \iint w(\rho,\theta,\zeta)\, d\theta\, d\zeta$$

$$\rightarrow \int d\rho \sum_{i=1}^{N_T} \sum_{j=1}^{N_Z} w(\rho,\theta_{i-1/2},\zeta_{j-1/2})\, \Delta\theta\, \Delta\zeta\ , \tag{51a}$$

where $\Delta\theta = 2\pi/N_T$, $\Delta\zeta = 2\pi/N_Z$ (N_T and N_Z are the number of discrete θ and ζ mesh points, respectively), $\theta_{i-1/2} = (i - 1/2)\,\Delta\theta$, $\zeta_{j-1/2} = (j - i/2)\,\Delta\zeta$, and

$$w = RG\left(\frac{|B|^2}{2} + \frac{p}{\gamma - 1}\right) \tag{51b}$$

is the energy density functional evaluated at the angular half-mesh points, where $\sqrt{g} = RG$, $p = M(\rho)(V')^{-\gamma}$, and

$$V'(\rho) = \sum_i \sum_j \sqrt{g}(\rho, \theta_{i-1/2}, \zeta_{j-1/2})\ \Delta\theta\ \Delta\zeta\ . \tag{51c}$$

A rectangle integration rule accurate to second order in $\Delta\theta$ and $\Delta\zeta$ was used in Eq. (51a). Because this rule preserves the discrete orthogonality of the trigonometric functions, it is more accurate[14] in the present problem than certain nominally higher-order schemes (e.g., Simpson's rule or Gaussian quadrature). If there are M theta modes and N zeta modes in the spectrum of R, Z, and λ, then $N_T = 2M + 1$ and $N_Z = 2N + 1$ are the minimum number of points required in the sum in Eq. (51a). (This estimate assumes that the modes are consecutive and counts $M \geq 0$, $N \geq 0$.)

The Fourier analysis of the coordinates R, Z, and λ appearing in the energy density w permits an <u>exact</u> evaluation of w at the half-mesh points $(\theta_{i-1/2}, \zeta_{j-1/2})$. It is this interpolation property of the trigonometric functions, together with the application of fast transform techniques, that makes harmonic analysis desirable even for the very nonlinear equilibrium problem under consideration here.[15]

What remains in Eq. (51a) is now a one-dimensional integration in ρ. Consider the set of N_ρ discrete radial mesh points (nodes) $\rho_k \equiv (k - 1)\Delta\rho$ for $k = 1, \ldots, N_\rho$, where $\Delta\rho = (N_\rho - 1)^{-1}$. The Fourier coefficients $X_\alpha^{mn}(\rho = \rho_k)$ for $\alpha = (R,\lambda,Z)$ will be denoted $X_\alpha^{mn}(k)$. They are the <u>nodal amplitudes</u>, which are to be obtained as the solution to the discrete force equations. In analogy with the angle discretization in Eq. (51), it is useful to introduce the radial half-mesh points $\rho_{k+1/2} = (\rho_k + \rho_{k+1})/2$, for $k = 1, \ldots, N_\rho - 1$. Then, the ρ integration in Eq. (51a) becomes

$$W = \sum_{k=1}^{N_\rho - 1} \sum_{i=1}^{N_T} \sum_{j=1}^{N_Z} w(\rho_{k+1/2}, \theta_{i-1/2}, \zeta_{j-1/2})\ \Delta\rho\ \Delta\theta\ \Delta\zeta\ . \tag{52}$$

Henceforth, for brevity, the angular subscripting is suppressed. To evaluate w at the radial half-mesh points, central sum and difference formulas[18] can be used: $X_\alpha(k + 1/2) = [X_\alpha(k) + X_\alpha(k + 1)]/2$ and $X'_\alpha(k + 1/2) = [X_\alpha(k + 1) - X_\alpha(k)]/\Delta\rho$. Since w depends only on X_α and X'_α, but no higher-order radial derivatives, these relations are sufficient to discretize w.

The discrete forces are obtained by taking the time derivatives of the nodal amplitudes $X_\alpha^{mn}(k,t)$ appearing in the discrete form for W, in exact analogy with the procedure developed in Sec. III for the continuous case. The result is not unique, since several radial discretizations of w, all of which agree to $O(\Delta\rho^2)$, are possible. The particular discrete form for w used here was chosen to minimize the radial coupling between the nodal amplitudes, which is desirable both for numerical stability and for minimizing truncation errors.[4] In the pressure contribution to W [the second term in Eq. (51b)], V′ is differenced to conserve the volume, thus preserving the feature that the MHD forces depend on p only through $\partial p/\partial\rho$. This is accomplished by introducing $U = R^2/2$ and writing

$$V'(k + 1/2) = \sum_i \sum_j (U_\theta Z_\rho - U_\rho Z_\theta)^{k+1/2} \Delta\theta \, \Delta\zeta \, , \tag{53}$$

where each term on the right of Eq. (53) is evaluated individually at $\rho_{k+1/2}$; for example, $U_\theta(k + 1/2) = RR_\theta(k) + RR_\theta(k + 1)$.

The quantity $\sqrt{g}|B|^2$ appearing in the magnetic field energy $W_B = W - W_p$ is evaluated at $\rho_{k+1/2}$ as follows:

$$(\sqrt{g}|B|^2)^{k+1/2} = \left[\frac{(\Phi')^2}{\mu_0 G}\right]^{k+1/2} \left[\frac{b^2(k) + b^2(k + 1)}{2}\right] , \tag{54a}$$

where

$$G(k + 1/2) = (R_\theta Z_\rho - R_\rho Z_\theta)^{k+1/2}, \tag{54b}$$

$$b^2(k) = \left(b_\theta^2 \hat{g}_{\theta\theta} + 2b_\theta b_\zeta \hat{g}_{\theta\zeta} + b_\zeta^2 \hat{g}_{\zeta\zeta}\right)^k . \tag{54c}$$

$\hat{g}_{ij}(k) \equiv g_{ij}(k)/R(k)$ are the normalized metric coefficients, $b_\theta(k) = \iota(k) - \lambda_\zeta(k)$, $b_\zeta(k) = 1 + \lambda_\theta(k)$, and $\iota(k)$ is the discrete rotational transform profile. The ratio Φ'/G, which is proportional to the toroidal magnetic field, has been differenced on the half-grid to preserve the slowly varying radial behavior of this physical variable.

Using these expressions to complete the discretization of W in Eq. (51a) and taking a time derivative yields

$$\frac{dW}{dt} = -\sum_{i,j,k} [A_\alpha(k) - imB_\alpha(k) + inC_\alpha(k)]\Psi_{mn}\dot{X}_\alpha^{mn}(k)\ \Delta\rho\ \Delta\theta\ \Delta\zeta , \tag{55}$$

where $\Psi_{mn} \equiv \exp[i(m\theta_{i-1/2} - n\zeta_{j-1/2})]$. The coefficients A, B, and C at interior radial mesh points are

$$A_R(k) = \frac{(Z_\theta P)^{k+1/2} - (Z_\theta P)^{k-1/2}}{\Delta\rho} + (RZ_\theta)^k p'(k) + \Phi_k^* \left[\frac{b^2(k)}{2R(k)} - b_\zeta^2(k)\right] , \tag{56a}$$

$$B_R(k) = -\frac{1}{2}\left[(Z_\rho P)^{k+1/2} + (Z_\rho P)^{k-1/2}\right] + (b_\theta b_R)^k , \tag{56b}$$

$$C_R(k) = (b_\zeta b_R)^k , \tag{56c}$$

$$A_Z(k) = \frac{(R_\theta P)^{k-1/2} - (R_\theta P)^{k+1/2}}{\Delta\rho} - (RR_\theta)^k p'(k) , \tag{56d}$$

$$B_Z(k) = \frac{1}{2}\left[(R_\rho P)^{k+1/2} + (R_\rho P)^{k-1/2}\right] + (b_\theta b_Z)^k \ , \tag{56e}$$

$$C_Z(k) = (b_\zeta b_Z)^k \ , \tag{56f}$$

$$A_\lambda(k) = 0 \ , \tag{56g}$$

$$B_\lambda(k) = \hat{\Phi}_k(b_\theta \hat{g}_{\theta\zeta} + b_\zeta \hat{g}_{\zeta\zeta})^k \ , \tag{56h}$$

$$C_\lambda(k) = -\hat{\Phi}_k(b_\theta \hat{g}_{\theta\theta} + b_\zeta \hat{g}_{\theta\zeta})^k \ . \tag{56i}$$

Here,

$$\Phi_k^* = \frac{1}{2\mu_0}\left\{\left[\frac{(\Phi')^2}{G}\right]^{k+1/2} + \left[\frac{(\Phi')^2}{G}\right]^{k-1/2}\right\} \ , \tag{57a}$$

$$\hat{\Phi}_k = \frac{1}{4\mu_0}\left[(\Phi')^{k-1/2} + (\Phi')^{k-1/2}\right]\left[\left(\frac{\Phi'}{G}\right)^{k+1/2} + \left(\frac{\Phi'}{G}\right)^{k-1/2}\right] \tag{57b}$$

$$b_R(k) = \frac{\Phi_k^*}{R(k)}\,(b_\theta R_\theta + b_\zeta R_\zeta)^k \ , \tag{57c}$$

$$b_Z(k) = \frac{\Phi_k^*}{R(k)}(b_\theta Z_\theta + b_\zeta Z_\zeta)^k \ , \tag{57d}$$

$$P^{k+1/2} = \frac{1}{4\mu_0}\left[\left(\frac{\Phi'}{G}\right)^2\right]^{k+1/2}\left[b^2(k) + b^2(k+1)\right] \ , \tag{57e}$$

The discrete variational procedure yields Φ_k^*, instead of $\hat{\Phi}_k$, in Eqs. (56h,i). This departure from the rigorous variational result is introduced to preserve the correct asymptotic behavior for the discretized λ as $\rho \to 0$.

At the origin, the correct discrete expressions for the forces can be obtained by integrating Eq. (18) from $\rho = 0$ to $\rho = \Delta\rho/2$. The asymptotic forms for R, Z, and λ at the magnetic axis, which were derived in Sec. V, can then be used to obtain the following expressions:

$$A_R(1) = \frac{2(Z_\theta P)^{\frac{3}{2}}}{\Delta\rho} + \Phi_1^* \left[\frac{\hat{g}_{\zeta\zeta}(1)}{2R(1)} - 1\right] , \tag{58a}$$

$$C_R(1) = \frac{\Phi_1^*}{R(1)} R_\zeta(1) \quad , \tag{58b}$$

$$A_Z(1) = \frac{2(R_\theta P)^{\frac{3}{2}}}{\Delta\rho} , \tag{58c}$$

$$C_Z(1) = \frac{\Phi_1^*}{R(1)} Z_\zeta(1) , \tag{58d}$$

where

$$\Phi_1^* = \frac{1}{2\pi} \left[\frac{(\Phi')^2}{G}\right]^{\frac{3}{2}} \tag{58e}$$

and $P^{3/2}$ is given by Eq. (57e) for $k = 1$. Note that $b^2(1) = \hat{g}_{\zeta\zeta}(1)$, and $B_R(k)$ and $B_Z(k)$ do not contribute to the $m = 0$ force components [since they are multiplied by (im) in Eq. (55)]. The result in Eq. (58) differs from the variational discretization by the extra factor of 2 appearing in the radial derivative terms of A_R and A_Z. This discrepancy can be traced to the inadequacy of the differencing scheme for $|B|^2$ in Eq. (54a) as $\rho \to 0$.

At the plasma boundary $\rho_k = 1$, either R and Z are prescribed for a fixed boundary equilibrium, or $P(b) = R(b)|\nabla\Phi|^2(b)/2\mu_0$ (where b denotes the boundary) can be used in Eq. (56) for a free boundary equilibrium. The λ force may be obtained by extrapolating the value of the toroidal field to the boundary. Then B_λ and C_λ have the forms given in Eq. (56), with $\hat{\Phi}_k$ replaced by

$$\hat{\Phi}(b) = \frac{(\Phi'_b)^2}{\mu_0 G(b)} . \tag{59}$$

where $\Phi'_b = 1.5\Phi'(N_\rho - 1/2) - 0.5\Phi'(N_\rho - 3/2)$, $G(b) = R_\theta(b)Z_\zeta(b) - R_\rho(b)Z_\theta(b)$, where $Z_\rho(b) \simeq Z_\rho(N_\rho - 1/2)$ and $R_\rho(b) \simeq R_\rho(N_\rho - 1/2)$.

Comparing Eqs. (56)-(58) with Eq. (18), it is apparent that A_α arises from the ρ derivative terms in the MHD forces (together with the centrifugal force in F_R), and B_α and C_α arise from the total θ and ζ derivative terms, respectively. The coefficient of $\dot{X}^{mn}_\alpha(k)$ in Eq. (55) yields the following nodal equations for the discrete Fourier-transformed MHD forces:

$$(V'_j)F^{mn}_\alpha(k) = A^{mn}_\alpha(k) + imB^{mn}_\alpha(k) - inC^{mn}_\alpha(k) , \tag{60}$$

where $A^{mn}_\alpha(k) \equiv \sum_{i,j} A_\alpha(k)\Psi^*_{mn}\,\Delta\theta\,\Delta\zeta$ is the discrete Fourier transform of $A_\alpha(k)$.

IX. GALERKIN METHOD FOR MAGNETIC AXIS

Because of the singular behavior of the force equations in the neighborhood of the magnetic axis, it was necessary in the previous section to give special consideration to the discretization process as $\rho \to 0$. As the number of Fourier mode amplitudes increases, there is a greater sensitivity to small numerical errors in the position of the axis, as well as the plasma shift, so that the convergence of the descent algorithm is adversely effected. Improved numerical stability of the descent iteration can be realized by applying the Galerkin method to the axis shift components,

$$R_0(\zeta,\rho) \equiv \frac{1}{2\pi}\int R\, d\theta = \sum_n R^{0n}(\rho)\exp(-in\zeta) , \tag{61a}$$

$$Z_0(\zeta,\rho) \equiv \frac{1}{2\pi}\int Z\, d\theta = \sum_n Z^{0n}(\rho)\exp(-in\zeta) , \tag{61b}$$

comprising the $m = 0$ Fourier components of R and Z. The method consists of expanding the Fourier amplitudes R^{0n} and Z^{0n} in a polynomial series in ρ, rather than discretizing them on a radial mesh. The improved numerical properties associated with this Galerkin procedure arise from two features of the method: (i) the magnetic axis $R_0(\zeta,0)$, $Z_0(\zeta,0)$ is now determined by an average force balance over ρ, rather than by the force at the singular point $\rho = 0$ alone; and (ii) the radial variation of R_0, Z_0 will be smooth as a function of ρ, thus guaranteeing a well-behaved Jacobian $\sqrt{g}$ (which is strongly effected by the radial gradients of R_0, Z_0).

Let X_j^{0n} denote R^{0n} or Z^{0n} for $j = 1$ or 2, respectively. Then

$$X_j^{0n}(\rho) = \sum_{k=0} c_{nk}^j u_k(\rho) , \tag{62a}$$

where $u_k(\rho) = \sqrt{(4k+1)}P_{2k}(\rho)$ and P_{2k} is the Legendre polynomial of order 2k. This choice of basis functions was motivated by noting that $u_k'(0) = 0$ satisfies the boundary condition Eq. (27b) at the magnetic axis. The u_k are orthonormal polynomials on the interval $\rho = [0,1]$ with unit weight function. Since the boundary condition $X_j^{0n}(1) = X_{jb}^{0n}$ may be prescribed, the c_{nk}^j are not independent but satisfy $\sum_{k=0} \sqrt{(4k+1)}c_{nk}^j = X_j^{0n}(1)$. Using this relation to eliminate c_{n0}^j yields an unconstrained Galerkin expansion for X_j^{0n}:

$$X_j^{Vn}(\rho) = X_j^{Vn}(1) + \sum_{k=1} c_{hk}^{j} 0_k(\rho) \ , \tag{62b}$$

where $0_k(\rho) = \sqrt{(4k+1)}[P_{2k}(\rho) - 1]$. Inserting this expansion into Eq. (21a) for $\dot{W}$ yields descent equations for c_{hk}^{j}:

$$\dot{c}_{hk}^{j} = \int_0^1 0_k F_j^{Vn} \, dV \ . \tag{63}$$

Obviously, the expansion coefficients are determined by radially weighted averages of the MHD residual forces.

For the examples discussed in the next section, the Galerkin method has been used when mode convergence studies, requiring many Fourier modes, were performed. In all instances examined so far, the Galerkin approach has been as accurate as, but more stable than, the discretization method when increasing numbers of Fourier modes are retained. Also, good radial resolution is generally achieved by retaining only two or three expansion coefficients in the series, Eq. (62b).

X. NUMERICAL EXAMPLES

Some numerical results obtained using the method described in the previous sections are now presented. In all the examples, the effect of the angle renormalization parameter λ is substantial. A symmetry property of particular prevalence in stellarator designs, which permits a substantial reduction in the number of equilibrium equations, has been used to obtain these numerical results. Many systems of practical interest possess at least one toroidal plane ($\phi = 0$, specifically) where the coil symmetry imposes a flux surface shape with vertical symmetry. In this plane, $R(\rho,\theta,0) = R(\rho,-\theta,0)$ and $Z(\rho,\theta,0) = -Z(\rho,-\theta,0)$. By analytic

continuation, this symmetry property implies the following Fourier series for R,Z for all values of ϕ:

$$R(\rho,\theta,\phi) = \sum_{m,n} R^{mn}(\rho)\cos(m\theta - n\phi) , \tag{64a}$$

$$Z(\rho,\theta,\phi) = \sum_{m,n} Z^{mn}(\rho)\sin(m\theta - n\phi) . \tag{64b}$$

Thus, half the possible terms in the general Fourier expansion of R,Z have been eliminated by symmetry. Furthermore, by examining the structure of the Γ_λ operator defined in Eq. (14b), it is possible to infer that

$$\lambda(\rho,\theta,\phi) = \sum_{m,n} \lambda^{mn}(\rho)\sin(m\theta - n\phi) . \tag{64c}$$

Figures 2-4 show the flux surfaces, normalized Fourier amplitudes, and residual decay, respectively, for the particular 2-D Solov'ev equilibrium discussed in Ref. 4. With a radial mesh of 10-20 points, a discretization error of less than 0.1% in the value of $R_0(0)$ (which should be 4) was obtained using more than two harmonics for R, Z, and λ. For the example shown, a total of 12 harmonic amplitudes was retained (although a minimum of 6 harmonics produces essentially the same flux surface configurations). In Fig. 2, the solid lines represent the magnetic surfaces and the dashed lines correspond to constant θ contours. Note that after the first 100 iterations the energy has already converged to within three significant figures, whereas the residuals $|F^2| \equiv \int F^2\, dV$ (which are normalized to W) continue to decay at a more or less uniform rate.

Figures 5-7 illustrate the same features for a high-beta ($\langle\beta\rangle = 3\%$), axisymmetric, D-shaped plasma. The pressure profile was taken to be $p = p_0(1 - \rho^2)^2$ and the rotational transform was given by $\iota = 1 - 0.67\rho^2$.

Because the Jacobian for the D-shaped configuration is not uniform with respect to the poloidal angle θ, there is a substantial decrease in the rate of residual decay in this case compared with the Solov'ev equilibrium for which $\partial\sqrt{g}/\partial\theta = 0$ [see Eq. (42)]. The figures correspond to a total of 12 poloidal harmonics, although convergence has been achieved with up to 30 harmonics. This limited convergence study indicates that after a certain minimum number of harmonics is present, the values of the lowest order harmonics seem to remain invariant to the addition of further harmonics.

Figures 8–10 present the flux surface and residual decay for the heliotron model configuration,[16] which has an outer boundary ($\rho = 1$)

$$R = 10 - \cos\theta - 0.3\cos(\theta - P\zeta) \ , \tag{65a}$$

$$Z = \sin\theta - 0.3\sin(\theta - P\zeta) \ , \tag{65b}$$

where $P = 19$ is the number of field periods. A total of 18 mode amplitudes (6 modes each for R, Z, and λ, corresponding to all combinations of $m = 0$, 1, 2 and $n = 0$, P) was used to obtain the equilibrium configurations shown. Here, the pressure is $p = p_0(1 - \rho^2)^2$, and $\iota = 0.5 + 1.5\rho^2$. The low-beta result shows the approximate vacuum topology, whereas at high beta ($\langle\beta\rangle = 2\%$), a substantial Shafranov shift $\Delta \sim 0.2$ is apparent. To obtain the residual decay shown in Fig. 10 for $\langle\beta\rangle = 2\%$ took about 32 s of cpu time on the CRAY computer. The results of a beta scan are summarized in Fig. 11, where the average toroidal shift $\Delta R = (R_{00} - 19)$ is displayed vs $\langle\beta\rangle$. This is in approximate agreement with the free boundary calculations reported in Ref. 16.

Finally, Figs. 12 and 13 represent the flux surfaces for the Advanced Toroidal Facility (ATF)[17] model configuration, with an outer boundary

$$R = 2.05 - 0.29 \cos\theta + 0.09 \cos(\theta - P\zeta) + 0.125[\cos 2\theta - \cos(2\theta - P\zeta)] , \quad (66a)$$

x $$Z = 0.29 \sin\theta + 0.09 \sin(\theta - P\zeta) + 0.00675[\sin 2\theta - \sin(2\theta - P\zeta)] , \quad (66b)$$

where $P = 12$. The pressure was chosen to be $p = p_0(1 - \rho^2)^2$, and $\iota = 0.35 + 0.65\rho^2$. In Eq. (66), the $(\cos\theta, \sin\theta)$ terms produce an axisymmetric circular plasma and the $[\cos(\theta - P\zeta), \sin(\theta - P\zeta)]$ terms represent a helically varying elliptical distortion. The last terms in Eq. (66) describe the D-shaped distortion of the plasma most notable in Figs. 12 and 13 at $P\zeta = \pi$. At the higher $\langle\beta\rangle$ value, a marked helical distortion ($\cos P\theta$, $\sin P\theta$ terms) of the magnetic axis develops, even though there is no pure helical modulation of the boundary surface. Figure 14 shows the mean toroidal axis shift $\Delta R = (R_{00} - 2.05)$ vs $\langle\beta\rangle$ for this ATF model, which is in good agreement with the results obtained in Ref. 17.

ACKNOWLEDGMENTS

The authors would like to acknowledge useful discussions with R. M. Wieland, A. Schlüter D. J. Sigmar, J. Smith, S. Jardin and C. Handy. D. J. Danzy deserves a special note of appreciation for her dedication in preparing this manuscript.

APPENDIX A: ALTERNATIVE CALCULATION OF THE MHD FORCE

The MHD residual force $\vec{F}$ defined in Eq. (1a) can be decomposed as

$$\vec{F} = \nabla\left(p + \frac{|B|^2}{2\mu_0}\right) - \frac{\vec{B} \cdot \nabla\vec{B}}{\mu_0}$$

$$= \nabla\alpha_i \frac{\partial P}{\partial \alpha_i} - \frac{1}{\mu_0}\left(B^\theta \frac{\partial \vec{B}}{\partial \theta} + B^\zeta \frac{\partial \vec{B}}{\partial \zeta}\right) , \qquad (A1)$$

where $\vec{\alpha} = (\rho,\theta,\zeta)$ and $P = p + |B|^2/2\mu_0$. The contravariant cylindrical coordinate basis vectors are $\vec{e}^j$, where $\vec{e}^R = \nabla R = \cos\phi i_x + \sin\phi i_y$, $\vec{e}^\phi = \nabla\phi = (-\sin\phi i_x + \cos\phi i_y)R^{-1}$, and $\vec{e}^Z = \nabla Z$. Here, i_x and i_y are fixed Cartesian vectors in the R,Z plane. Then, the covariant components of $\vec{F}$ are $\vec{e}_k = R\vec{e}^i \times \vec{e}^j$. For example, $\vec{e}_R = \nabla R$. Thus,

$$F_R \equiv \nabla R \cdot \vec{F}$$

$$= \frac{\partial \alpha_i}{\partial R}\frac{\partial P}{\partial \alpha_i} - \frac{1}{\mu_0}\left(B^\theta \frac{\partial B_R}{\partial \theta} + B^\zeta \frac{\partial B_R}{\partial \zeta}\right) + \vec{B} \cdot \left(\frac{B^\theta}{\mu_0}\frac{\partial}{\partial \theta} + \frac{B^\zeta}{\mu_0}\frac{\partial}{\partial \zeta}\right)\nabla R . \qquad (A2)$$

For the choice of toroidal coordinates $\zeta = \phi$, note that $\partial\nabla R/\partial\theta = 0$ and $\partial\nabla R/\partial\zeta = R\nabla\phi$. Thus, Eq. (A2) becomes

$$F_R = \frac{\partial \rho}{\partial R}\frac{\partial P}{\partial \rho} + \frac{\partial \theta}{\partial R}\frac{\partial P}{\partial \theta} - \frac{1}{\mu_0}\left(B^\theta \frac{\partial B_R}{\partial \theta} + B^\zeta \frac{\partial B_R}{\partial \zeta}\right) + \frac{R(B^\zeta)^2}{\mu_0} . \qquad (A3)$$

Multiplying F_R by $-\sqrt{g}$, using Eq. (12e) for the adjoint components $\partial\alpha_i/\partial R$,

and noting that $\nabla \cdot \vec{B} = 0$ implies $\partial(\sqrt{g}B^{\theta})/\partial\theta + \partial(\sqrt{g}B^{\zeta})/\partial\zeta = 0$ yields the expression for F^R given in Eq. (18a).

An expression for F^Z in agreement with Eq. (18b) is obtained in a similar manner by considering the $\vec{e}_Z = \nabla Z$ component of $\vec{F}$.

APPENDIX B: OPTIMAL CHOICE FOR THE POLOIDAL ANGLE

The rate at which a magnetic flux surface is traversed in the poloidal direction can be independent of its shape. This leads to the interdependence of the MHD forces F_R, F_Z, and F_λ when the renormalization parameter λ is introduced. This degeneracy may be resolved by specifying the poloidal angle θ. Several choices for θ have been discussed in the literature.[4,5,7,18] In this appendix, it is argued that the requirement of rapid convergence for the Fourier moment expansions of R and Z selects a particular angle θ that has not been previously considered.

One choice[4] for θ is a polar representation for which $\theta = \tan^{-1}(\bar{Z}/\bar{R})$, where $(\bar{R}, \bar{Z})$ are local Cartesian coordinates (in the plane ϕ = const) measured from the magnetic axis. In this system, Eq. (16) is replaced by a single equation $\dot{r} \sim F_\rho$, where $r = (\bar{R}^2 + \bar{Z}^2)^{1/2}$ is the polar radius. Because $r(\rho,\theta,\zeta)$ must be a single-valued function of the flux coordinates, this representation is limited to starlike domains (or boundary shapes that can be mapped into starlike domains) and cannot describe, for example, strongly pinched surfaces that might appear in a plasma preceding the development of magnetic islands. In addition, the polar angle θ may not lead to a rapidly convergent Fourier expansion of r. (This difficulty poses no problem in Ref. 4, where Fourier analysis is not used.) For example, an elliptical flux surface $\bar{R}^2 + \bar{Z}^2/\kappa^2 = 1$ becomes (for $\kappa \geq 1$) $r = [1 - (1 - \kappa^{-2})\sin^2\theta]^{-1/2}$, which develops a significant Fourier spectrum as κ departs from unity. The same problem exists for certain other angle choices. For example, the angle producing equal arc lengths around a flux surface requires $\partial g_{\theta\theta}/\partial\theta = 0$ but can lead to a substantial Fourier spectrum even for the simplest noncircular geometric shapes.

To avoid the restriction to starlike domains imposed on the polar system, the cylindrical system (R,ϕ,Z) was introduced in Sec. III. In this system, a natural unique choice[7,18] for the poloidal angle is $\theta = \theta^*$, where θ^* is the angle that, together with $\zeta = \phi$, defines a straight magnetic field line coordinate system. Although this choice for θ is adequate in the context of Ref. 18, where the MHD equilibrium equations are solved on a Lagrangian grid, it is generally inappropriate for use in conjunction with Fourier analysis. (An explicit analytic example of this is given in Sec. VI.) The poor convergence properties associated with θ^* may be understood by considering a fixed plasma boundary with the following finite parametric representation:

$$R_b(\theta,\zeta) = \sum_{m=0}^{M_R} \sum_{n=-N_R}^{N_R} R^{mn}\cos(m\theta - n\zeta) \ , \tag{B1a}$$

$$Z_b(\theta,\zeta) = \sum_{m=0}^{M_Z} \sum_{n=-N_Z}^{N_Z} Z^{mn}\sin(m\theta - n\zeta) \ . \tag{B1b}$$

It is assumed that Eq. (B1) is the most economical series representation of the boundary, in the sense that any periodic displacement of θ increases the total number of harmonics, $M_R N_R + M_Z N_Z$. Note that the shape of the boundary, at a fixed toroidal angle ζ, is invariant to such displacements, which merely change the rate at which the boundary is traversed as θ increases. In general, the parametric (geometric) angle θ in Eq. (B1) does not coincide with θ^*. (Even if θ and θ^* agreed initially, it would be impossible to guarantee their equality as the plasma evolved toward equilibrium. This is because the operator F_λ, which determines the evolution of θ^*, depends on $\sqrt{g}$, which is not a function of the boundary

coordinates alone.) Thus, in terms of $\theta^* = \theta + \lambda_b^*(\theta^*,\zeta)$, where λ_b^* is a periodic function, Eq. (B1a) becomes (with a similar result for Z_b)

$$R_b(\theta^*,\zeta) = \sum\sum R^{mn}\cos[m(\theta^* - \lambda_b^*) - n\zeta]$$

$$= \sum_{m=0}^{M_R^*} \sum_{n=-N_R^*}^{N_R^*} R_*^{mn}\cos(m\theta^* - n\zeta) \ , \qquad (B2)$$

where $M_R^*N_R^* + M_Z^*N_Z^* > M_RN_R + M_ZN_Z$. Not only is the number of Fourier harmonics in general (substantially) increased in the θ^* system, but also the boundary coefficients R_*^{mn} are *no longer fixed during the energy minimization even for a fixed boundary equilibrium.* Rather, they undergo[18] periodic Lagrangian displacements along the boundary curve that are of the form $\delta R_b = R_\theta \dot{\lambda}$ and $\delta Z_b = Z_\theta \dot{\lambda}$, with $\dot{\lambda} = -F_\beta$. Thus, simply to conserve the outer boundary shape requires a large number of harmonics in the θ^* system. For these reasons, it is preferable to transform to the geometric coordinate system $\theta = \theta^* - \lambda_b^*$, where the boundary Fourier coefficients <u>can</u> be fixed and where the number of harmonics is minimized. Because of the large number of harmonics generated by the transformation to θ^* in Eq. (B2), it may be concluded that the development in Ref. 7, though technically correct, is of little practical importance.

Having transformed to θ at the boundary, it becomes necessary to extend this coordinate system into the plasma. This is exactly what Eq. (3a) accomplishes. The coefficients (R^{mn}, Z^{mn}) in Eq. (B1) are specified boundary values. This yields a unique transformation from θ^* to θ at the boundary. However, the transformation equation (3a) is not unique in the plasma interior, where the same flux surface can have an infinite number of parametric representations under the family of transformations

given by Eq. (3a). This underdetermination of θ is irrelevant in practice where only finite Fourier expansions are used to represent the equilibrium solutions. For finite-term series expansions of R and Z, there exists a unique poloidal angle θ (the geometric angle) that leads to the most accurate solution of the inverse equilibrium problem in the sense of convergence in the mean. (This conclusion concerning series economization follows from the Fourier-Bessel theory of finite-series approximation). We now demonstrate that the variational principle given in Sec. III is capable of determining the geometric poloidal angle as a result of the minimization process (with fixed boundary conditions). That is, the variational principle automatically performs the series economization when the angle renormalization parameter λ is retained. As a consequence, no constraint between the Fourier harmonics need be imposed ab initio whenever a finite-series approximation to R and Z is sought.

To prove this remarkable property of the variational equations it suffices to show that when $\lambda \neq 0$, the equations for $\dot{R}$ and $\dot{Z}$ are independent whenever finite Fourier series approximations for R and Z are used. Without loss of generality it may be assumed that $F_\lambda = 0$ can be satisfied by an appropriate choice of λ. Then Eq. (16) yields

$$\dot{R} = Z_\theta \bar{F}_\rho \,, \tag{B3a}$$

$$\dot{Z} = -R_\theta \bar{F}_\rho \,, \tag{B3b}$$

where $\bar{F}_\rho = RF_\rho$ is the 3-D inverse Grad-Shafranov operator. In the infinite mode number (continuous) limit, the underdetermination of θ is manifested in Eq. (B3) by the fact that $\dot{R}$ and $\dot{Z}$ are not independent equations. However, for a finite-series expansion of R and Z, and hence of R_θ and Z_θ,

the Fourier moments of the variational equation (B3) needed to extract the appropriate harmonics of $\dot{R}$ and $\dot{Z}$ yield exactly the correct number of independent equations for determining each of the harmonics of R and Z. This is due to the mode coupling produced by Z_θ and R_θ in Eq. (B3). (It is assumed that because of the strong nonlinearity of F_ρ, the harmonics of F_ρ are independent at least up to a mode number equal to the sum of the R and Z mode numbers. Also, since $\sqrt{g} \neq 0$, R_θ and Z_θ do not both vanish.)

Because Eq. (B3) is indeterminate in the continuous limit, it is probably ill-conditioned for finite but large mode numbers. Limited mode convergence studies (see Sec. IX) suggest that lack of uniqueness does not seem to produce any deleterious numerical effects when used in conjunction with the steepest descent method. This is probably due to the fact that the initial guess for (R^{mn}, Z^{mn}) is sufficient to yield a unique descent path and thus determines a unique poloidal angle even when many modes are present (up to 30 mode amplitudes have been successfully converged).

When a unique poloidal angle choice is desired, it is possible to scale λ from its value at the plasma boundary (which <u>is</u> unique) into the plasma. For example, $\lambda^{mn} = \rho^m \lambda_b^{mn}$ satisfies the boundary conditions for λ at $\rho = 0$ and $\rho = 1$. In this way, the renormalization features of λ are retained, while Eq. (B3) is no longer ill-conditioned.

APPENDIX C: DESCENT METHOD FOR THE VACUUM MAGNETIC FIELD

The consideration of the free plasma boundary in Sec. V.B led to the descent equation (31c) for the vacuum potential, with the boundary conditions $\vec{B}_v \cdot d\vec{S}_\rho = 0$ at $\rho = 1$ and $\vec{B}_v \cdot d\vec{S} = 0$ at the conducting wall. Equation (31c) is a 3-D parabolic equation for ν with homogeneous "flux" conditions on a moving boundary. The numerical problem of solving this equation in a time-varying, irregular domain can be overcome by transforming the cylindrical coordinates (R,ϕ,Z) in the vacuum region to polar coordinates (r,θ,ς) with $\varsigma = \phi$. Here $r = 0$ corresponds to the plasma boundary $[R_1(\theta,\varsigma) = R(\rho = 1,\theta,\varsigma),\ Z_1(\theta,\varsigma) = Z(\rho = 1,\theta,\varsigma)]$ and $r = 1$ is the coil (or wall) surface $[R_c(\theta,\varsigma),\ Z_c(\theta,\varsigma)]$. Thus,[4]

$$R = R_1(\theta,\varsigma,t) + r[R_c(\theta,\varsigma) - R_1(\theta,\varsigma,t)] , \tag{C1a}$$

$$Z = Z_1(\theta,\varsigma,t) + r[Z_c(\theta,\varsigma) - Z_1(\theta,\varsigma,t)] . \tag{C1b}$$

Note that the polar radius r is considered an independent variable in Eq. (C1) and therefore does not change during the variation of W_v. In this vacuum polar coordinate system, the variation of the vacuum energy becomes

$$\begin{aligned} -\dot{W}_v = & -\mu_0^{-1} \int_0^1 dr \int d\theta\, d\varsigma\, \sqrt{g_v} F_\nu (\dot{\nu} + \vec{v} \cdot \nabla\nu) \\ & + \mu_0^{-1} \int_{r=0} (\dot{\nu} + \vec{v} \cdot \nabla\nu) \vec{B}_v \cdot d\vec{S}_r , \end{aligned} \tag{C2}$$

where $d\vec{S}_r = \nabla r \sqrt{g_v}\, d\theta\, d\varsigma = d\vec{S}_\rho$. The surface contribution to S_i and the wall term in Eq. (30) are both unchanged by this coordinate transformation and have been omitted from Eq. (C2) for brevity. Now, $\dot{\nu} = \partial\nu/\partial t$ is taken at

fixed (r,θ,ς), and the convective speed due to the coordinate motion is $\vec{v} \cdot \nabla r \equiv \dot{r}$, $\vec{v} \cdot \nabla\theta \equiv \dot{\theta}$, and $\vec{v} \cdot \nabla\varsigma = 0$, where

$$\vec{v} \cdot \nabla r = \frac{R(1 - r)}{\sqrt{g_v}} (Z_\theta \dot{R}_1 - R_\theta \dot{Z}_1) , \tag{C3a}$$

$$\vec{v} \cdot \nabla\theta = - \frac{R(1 - r)}{\sqrt{g_v}} (Z_r \dot{R}_1 - R_r \dot{Z}_1) , \tag{C3b}$$

and $\dot{R}_1$ and $\dot{Z}_1$ are determined by the descent equations for the plasma moment amplitudes and the appropriate boundary conditions discussed in Sec. V. In the vacuum,

$$R_\theta = (1 - r)\frac{\partial R_1}{\partial\theta} + r\frac{\partial R_c}{\partial\theta} , \tag{C4a}$$

$$R_r = R_c - R_1 \tag{C4b}$$

(similar equations pertain for Z), and the Jacobian is

$$\sqrt{g_v} = R(R_\theta Z_r - R_r Z_\theta) . \tag{C4c}$$

Denoting the polar coordinates $(r,\theta,\varsigma) = (u_1,u_2,u_3)$, the 3-D Laplacian transforms in a conservative form as

$$F_\nu = \frac{1}{\sqrt{g_v}} \frac{\partial}{\partial u_i} \left(\sqrt{g_v} g_v^{ij} \frac{\partial\nu}{\partial u_j}\right) , \tag{C4d}$$

where the inverse metric tensor elements in the vacuum are

$$g_v^{ij} \equiv \nabla u_i \cdot \nabla u_j$$

$$= \frac{\partial u_i}{\partial R}\frac{\partial u_j}{\partial R} + \frac{1}{R^2}\frac{\partial u_i}{\partial \phi}\frac{\partial u_j}{\partial \phi} + \frac{\partial u_i}{\partial Z}\frac{\partial u_j}{\partial Z} \ . \qquad \text{(C4e)}$$

Explicit expressions for g_v^{ij} in terms of derivatives of R and Z with respect to u_i are [note that $g_v^{ij} = (\overleftrightarrow{g}_v^{-1})^{ij}$]:

$$g_v g_v^{11} = R^2 \hat{g}_{\theta\theta} + \Lambda_{\theta\zeta}^2 \ , \qquad \text{(C5a)}$$

$$g_v g_v^{12} = -R^2 \hat{g}_{r\theta} - \Lambda_{\theta\zeta}\Lambda_{r\zeta} \ , \qquad \text{(C5b)}$$

$$g_v g_v^{13} = \Lambda_{r\theta}\Lambda_{\theta\zeta} \ , \qquad \text{(C5c)}$$

$$g_v g_v^{22} = R^2 \hat{g}_{rr} + \Lambda_{r\zeta}^2 \ , \qquad \text{(C5d)}$$

$$g_v g_v^{23} = -\Lambda_{r\theta}\Lambda_{r\zeta} \ , \qquad \text{(C5e)}$$

$$g_v g_v^{33} = \Lambda_{r\theta}^2 \ . \qquad \text{(C5f)}$$

Here, $\hat{g}_{ij} = R_i R_j + Z_i Z_j$, $\Lambda_{ij} = R_i Z_j - R_j Z_i$, and $\sqrt{g_v} = -R\Lambda_{r\theta}$.

From Eq. (C2), the steepest descent equation for the vacuum potential, written in the polar coordinate system, becomes

$$\frac{\partial \nu}{\partial t} + \vec{v} \cdot \nabla \nu = F_\nu \ , \qquad \text{(C6)}$$

and the boundary condition $\vec{B}_v \cdot d\vec{S} = 0$ at r = 0 and r = 1 can be written

$$\sqrt{g_v} g_v^{1j} \frac{\partial \nu}{\partial u_j} = 0 \ . \qquad \text{(C7a)}$$

Since Eq. (C7a) is just the argument of the i = 1 ($u_1 = r$) derivative

appearing in F_ν, it is simple to incorporate this boundary condition into the finite-difference scheme for the vacuum. Similarly, the vacuum pressure term appearing in Eq. (31a) becomes

$$\left[|\sqrt{g}|\,\frac{\partial\rho}{\partial x_j}\left(\frac{|\nabla\nu|^2}{2\mu_0}\right)\right]_{\rho=1} = \left[\left(-RZ_\theta\delta_{jR} + RR_\theta\delta_{jZ}\right)\sum_{i,k=2}^{3}\frac{\bar{g}_\nu^{ik}}{2\mu_0}\frac{\partial\nu}{\partial u_i}\frac{\partial\nu}{\partial u_k}\right]_{r=0}, \quad \text{(C7b)}$$

where Eq. (C7a) was used to eliminate $\partial\nu/\partial r$ and $\bar{g}_\nu^{ij} = g_\nu^{ij} - g_\nu^{1i}g_\nu^{1j}/g_\nu^{11}$ may be explicitly evaluated as follows:

$$\bar{g}_\nu^{22} = \frac{R^2 + \hat{g}_{\zeta\zeta}}{g_\nu g_\nu^{11}}, \quad \text{(C8a)}$$

$$\bar{g}_\nu^{23} = \frac{-\hat{g}_{\theta\zeta}}{g_\nu g_\nu^{11}}, \quad \text{(C8b)}$$

$$\bar{g}_\nu^{33} = \frac{\hat{g}_{\theta\theta}}{g_\nu g_\nu^{11}}. \quad \text{(C8c)}$$

The solution of Eq. (C6) may be obtained in polar coordinates by expanding ν in a Fourier series:

$$\nu = -\frac{\mu_0}{2\pi}\left(I^\zeta\theta + I^\theta\zeta\right) + \sum_{m,n}\nu^{mn}(r)\exp[i(m\theta - n\zeta)]. \quad \text{(C9)}$$

Here, $I^\zeta \equiv \mu_0^{-1}\int \vec{B}_\nu \cdot d\vec{\ell}_\theta = \int \vec{J}\cdot\nabla\zeta\sqrt{g}\,d\rho\,d\theta$ is the net toroidal plasma current and $I^\theta \equiv \mu_0^{-1}\int \vec{B}_\nu \cdot d\vec{\ell}_\zeta$ is the poloidal current flowing in external conductors that intercept the plane $Z = 0$. These currents are fixed during

the variation of ν and should be chosen initially so that the surface-averaged toroidal and poloidal magnetic fields in the plasma and the vacuum are continuous at $\rho = 1$ (assuming p vanishes at the plasma edge). This choice will suppress the development of surface currents. Thus, from Ampère's law, Eq. (1b), it follows that

$$\mu_0 I^{\zeta} = \int_0^{2\pi} B_\theta \, d\theta \,, \tag{C10a}$$

$$\mu_0 I^{\theta} = \int_0^{2\pi} B_\zeta \, d\zeta \,, \tag{C10b}$$

where B_j are the covariant components of $\vec{B}$ evaluated at $\rho = 1$. In equilibrium, it follows from current conservation and $J^\rho = 0$ [Eq. (4e)] that I^{ζ} and I^{θ} as defined in Eq. (C10) are indeed constants, independent of both ζ and θ. Initially, however, B_θ and B_ζ may not satisfy Eq. (4e), so the remaining angle averages should be performed in Eq. (C10). When the currents I^{ζ} and I^{θ} are prescribed, Eq. (C10) can be inverted to determine $\Phi'(1)$ and $\chi'(1)$. The matrix of coefficients relating the currents to the fluxes (the inverse inductance matrix) is found from Eq. (C10) and Eq. (3) to be $(2\pi/\mu_0)\langle g_{ij}/\sqrt{g}\rangle$, where $(i, j) \in (\theta^*, \zeta)$ and the angle brackets denote a double angle average. Note that the relationship between total current and total plasma magnetic flux given in Eq. (C10) pertains only in the absence of surface currents. In general, since both the plasma fluxes and the currents are constant during the variation of W, a change in the inductance matrix implies the generation of surface currents needed to satisfy Ampère's law at $\rho = 1$.

Inserting Eq. (C9) into the vacuum energy descent equation (C2) yields

$$\frac{d\nu^{mn}(r,t)}{dt} = F_\nu^{mn} - \iint \exp[-i(m\theta - n\zeta)]\vec{v} \cdot \nabla\nu \, d\theta \, d\zeta \,, \tag{C11a}$$

where

$$F_\nu^{mn} = [V'(r)]^{-1} \int \sqrt{g_v} \exp[-i(m\theta - n\zeta)] F_\nu \, d\theta \, d\zeta \tag{C11b}$$

and $V'(r) = \iint d\theta \, d\zeta \sqrt{g_v}$. In Eq. (C11a), the convective terms are to be evaluated using Eq. (C9), noting that $\partial\nu/\partial\theta$ includes I^ζ as well as periodic terms. Similarly, ν_ζ contains a term arising from I^θ. Neglecting the surface terms in $\dot{W}_v$, which are zero for the natural boundary conditions, and using the descent equation (C11a) for the potential yields

$$\frac{dW_v}{dt} = \sum_{m,n} \int_0^1 V' |F_\nu^{mn}|^2 \, dr \,. \tag{C12}$$

Therefore, the vacuum potential energy is maximized and reaches a steady state if and only if the vacuum force F_ν^{mn} vanishes and the natural boundary conditions are satisfied.

The present treatment of the vacuum fields as a maximization problem coupled to the internal plasma equilibrium differs from the approach in Ref. 4. There, the vacuum pctential is relaxed quasi-statically for each shape change of the plasma boundary. In addition, here the currents I^ζ and I^θ are fixed during the descent of ν. If I^ζ and I^θ were allowed to vary in time in Eq. (C2), the additional term $-(\dot{I}^\zeta\chi_v + \dot{I}^\theta\Phi_v)/(2\pi\mu_0)$ would arise in $\dot{W}_v$, where χ_v and Φ_v are the total poloidal and toroidal vacuum fluxes, respectively. Therefore, in general, the maximization of the vacuum energy is inconsistent with fixing the vacuum fluxes when the representation $\vec{B}_v = -\nabla\nu$ is used.

REFERENCES

[1]M. D. Kruskal and R. M. Kulsrud, Phys. Fluids 1, 265 (1958).

[2]H. Grad, Phys. Fluids 7, 1283 (1964).

[3]R. Chodura and A. Schlüter, J. Comput. Phys. 37, 68 (1981).

[4]F. Bauer, O. Betancourt, and P. Garabedian, A Computational Method in Plasma Physics (Springer-Verlag, New York, 1978); Phys. Fluids 24, 48 (1981).

[5]L. L. Lao, S. P. Hirshman, and R. M. Wieland, Phys. Fluids 24, 1431 (1981).

[6]V. D. Pustovitov, V. D. Shafranov, L. E. Zakharov, L. M. Degtyarev, V. V. Drozdov, S. Y. Medvedev, and M. I. Mikhajlov, in Plasma Physics and Controlled Nuclear Fusion Research (International Atomic Energy Agency, Vienna, 1982), paper IAEA-CN-37/V-5.

[7]A. Bhattacharjee, J. C. Wiley, and R. L. Dewar, submitted to Phys. Fluids.

[8]J. M. Greene, J. L. Johnson, and K. E. Weimer, Phys. Fluids 14, 671 (1971).

[9]S. Hamada, Nucl. Fusion 1, 23 (1958).

[10]P. Garabedian, Math. Tables Aids Comput. 10, 183 (1956).

[11]G. D. Smith, Numerical Solution of Partial Differential Equations (Oxford University Press, London, 1965).

[12]L. S. Solov'ev, Sov. Phys.-JETP 26, 400 (1968).

[13]J. M. Ortega and W. C. Rheinboldt, Iterative Solution of Nonlinear Equations in Several Variables (Academic Press, New York, 1970), p. 21.

[14]P. J. Davis and P. Rabinowitz, Methods of Numerical Integration (Academic Press, New York, 1975), pp. 108 ff.

[15]S. A. Orszag, J. Comput. Phys. 37, 70 (1980).

[16]F. Bauer, O. L. Betancourt, P. R. Garabedian, and J. L. Shohet, IEEE Trans. Plasma Sci. PS-9, 239 (1981).

[17]J. F. Lyon, B. A. Carreras, J. H. Harris, J. A. Rome, R. A. Dory, L. Garcia, T. C. Hender, S. P. Hirshman, T. C. Jernigan, J. Sheffield, L. A. Charlton, R. H. Fowler, H. R. Hicks, J. A. Holmes, V. E. Lynch, B. F. Masden, D. L. Goodman, and S. A. Hokin, in Plasma Physics and Controlled Nuclear Fusion Research (International Atomic Energy Agency, Vienna, 1982), paper IAEA-CN-37/Q3.

[18]A. Schlüter and U. Schwenn, Comput. Phys. Comm. 24, 263 (1981).

FIGURE CAPTIONS

Fig. 1 Toroidal-cylindrical coordinate system.

Fig. 2 Flux surfaces for Solov'ev equilibrium $(R/4)^2 = 1 - (\rho/2)\cos\theta$, $Z = (\sqrt{10}/2)\sin\theta$, $p = (1 - \rho^2)/8$, and $\chi = \rho^2$.

Fig. 3 Normalized profiles $\bar{R}_m = R_{m0}/R_m^*$ and $\bar{Z}_m = Z_{m0}/Z_m^*$ for Solov'ev equilibrium, where $R_0^* = 3.999$, $R_1^* = 1.026$, $R_2^* = 0.088$, $Z_1^* = 1.58$, and $Z_2^* = 0.01$.

Fig. 4 Residual decay and change in energy as a function of iteration number for Solov'ev equilibrium.

Fig. 5 Flux surfaces for high-beta, D-shaped plasma, $\langle\beta\rangle \simeq 3\%$, with $R_b = 3.51 - \cos\theta + 0.108\cos 2\theta$, $Z_b = 1.47\sin\theta + 0.16\sin 2\theta$.

Fig. 6 Normalized profiles $\bar{R}_m = R_{m0}/R_m^*$ and $\bar{Z}_m = Z_{m0}/Z_m^*$ for high-beta, D-shaped plasma, with $R_0^* = 3.97$, $R_1^* = 1.00$, $R_2^* = 0.107$, $Z_1^* = 1.47$, and $Z_2^* = 0.16$.

Fig. 7 Residual decay and change in energy as a function of iteration number for the high-beta, D-shaped plasma.

Fig. 8 Low-beta ($\langle\beta\rangle = 0.1\%$) flux surfaces for heliotron model configuration; $R_b = 10 - \cos\theta - 0.3\cos(\theta - P\varsigma)$, $Z_b = \sin\theta - 0.3\sin(\theta - P\varsigma)$, with $p = 19$.

Fig. 9 High-beta ($\langle\beta\rangle = 2\%$) flux surfaces for heliotron model configuration.

Fig. 10 Residual decay for the high-beta heliotron configuration.

Fig. 11 Toroidal shift ΔR vs $\langle\beta\rangle$ for heliotron configuration.

Fig. 12 Moderate-beta ($\langle\beta\rangle = 2\%$) flux surfaces for ATF model configuration; $R_b = 2.05 - 0.29\cos\theta + 0.09\cos(\theta - P\varsigma) +$

$0.0125[\cos 2\theta - \cos(2\theta - P\zeta)]$, $Z_b = 0.29 \sin\theta + 0.09 \sin(\theta - P\zeta) +$ $0.0067[\sin 2\theta - \sin(2\theta - P\zeta)]$, with $P = 12$.

Fig. 13 High-beta ($\langle\beta\rangle = 8\%$) flux surfaces for ATF model configuration.

Fig. 14 Toroidal shift ΔR vs $\langle\beta\rangle$ for ATF configuration.

ORNL-DWG 83-2601 FED

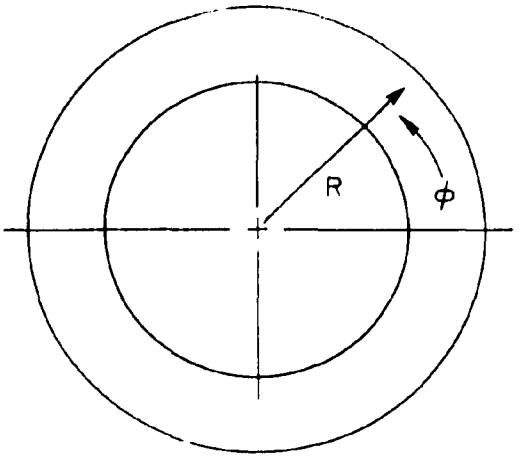

⊙ Z

TOROIDAL DOMAIN: TOP VIEW

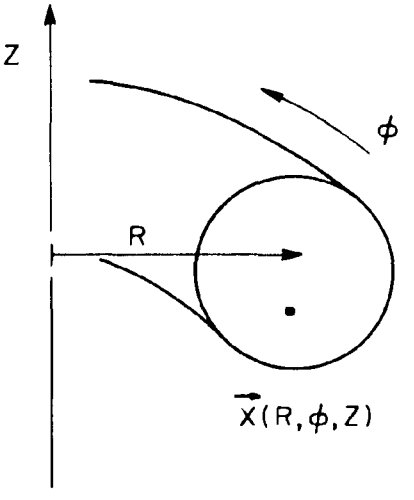

TOROIDAL DOMAIN: VIEW IN PLANE Z=CONSTANT

Fig. 1

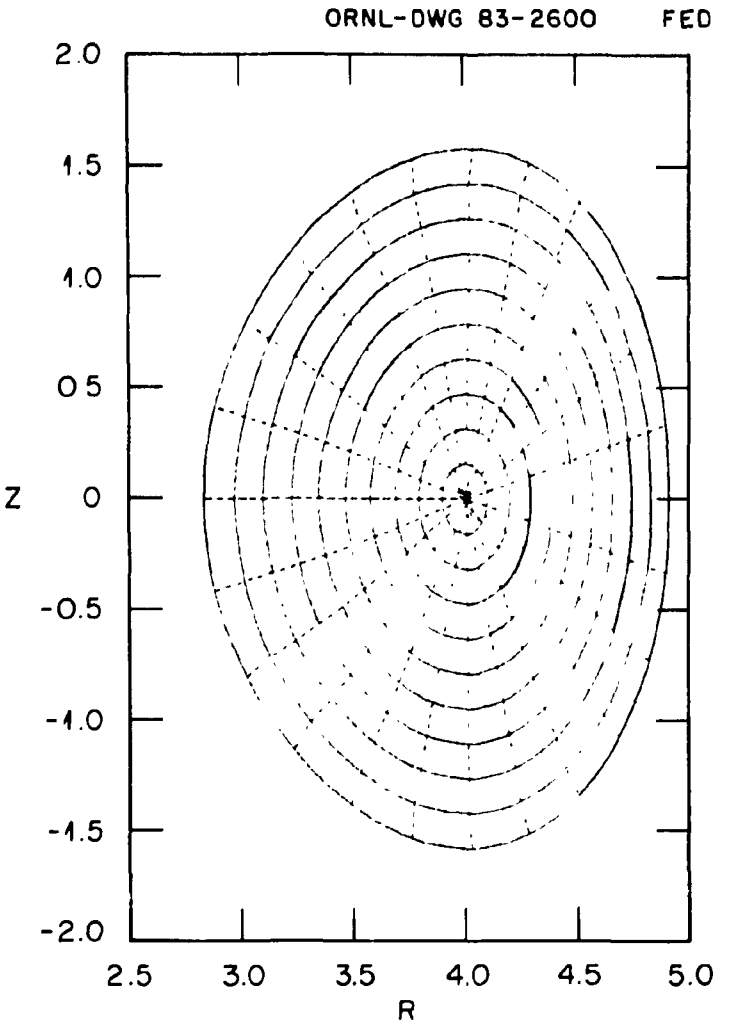

Fig. 2

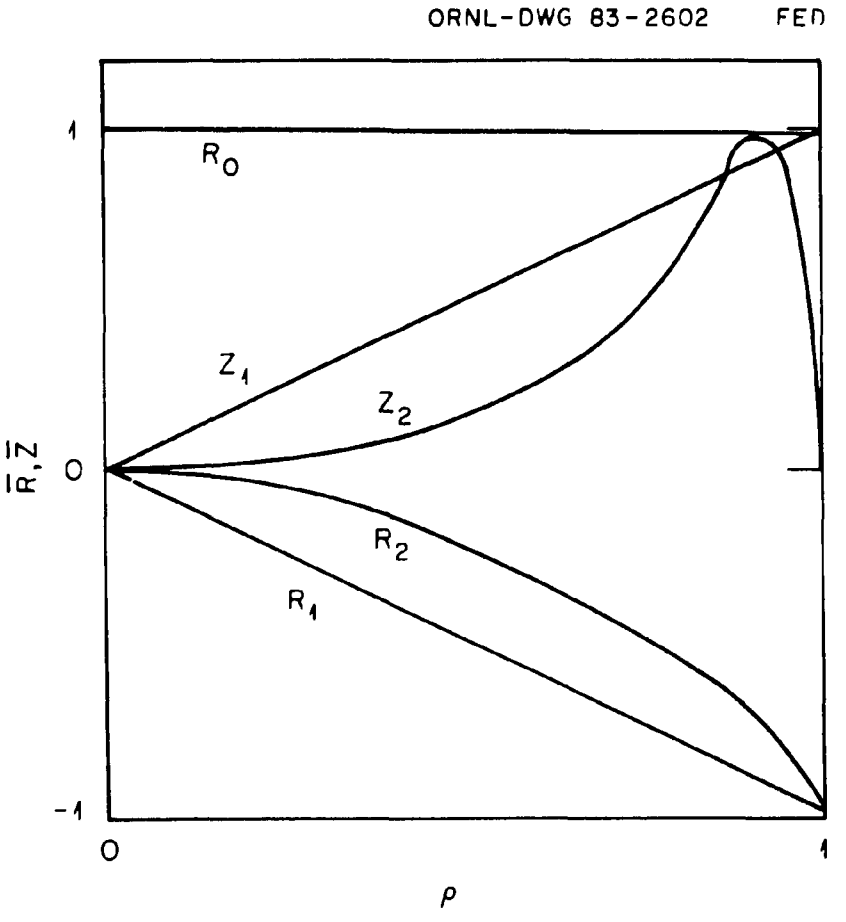

Fig. 3

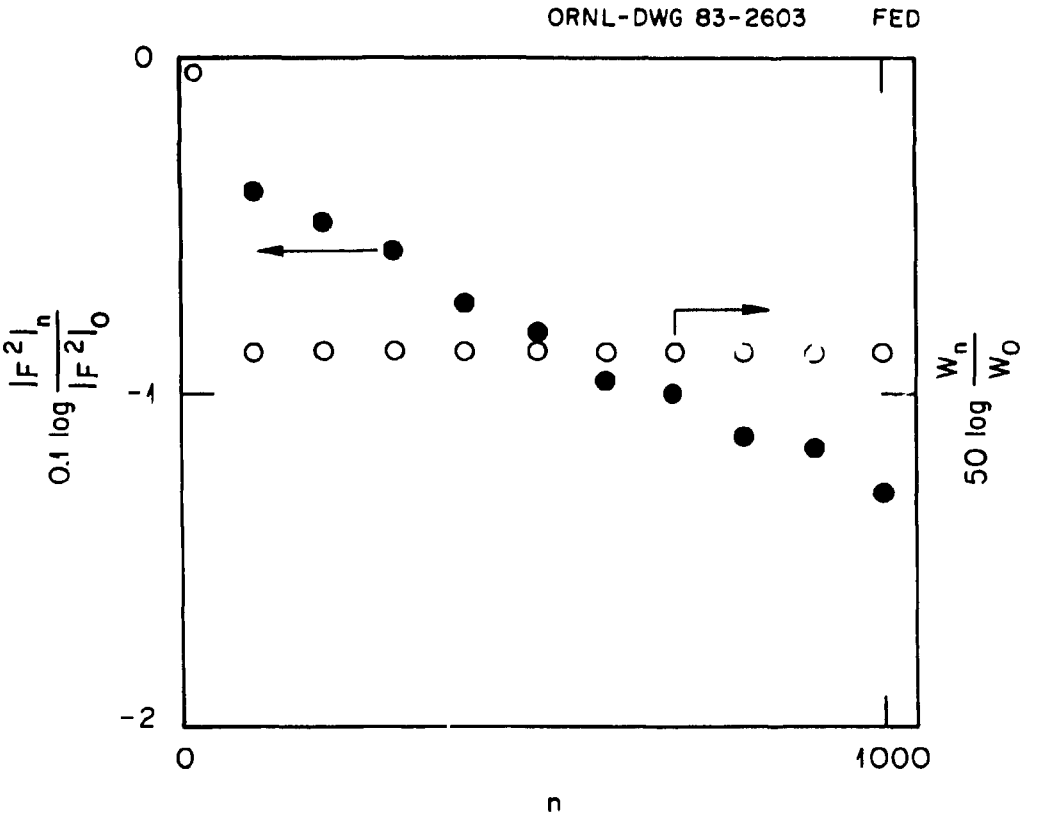
ORNL-DWG 83-2603 FED
0
-1
-2
0
1000
n
$0.1 \log \frac{|F^2|_n}{|F^2|_0}$
$50 \log \frac{W_n}{W_0}$

Fig. 4

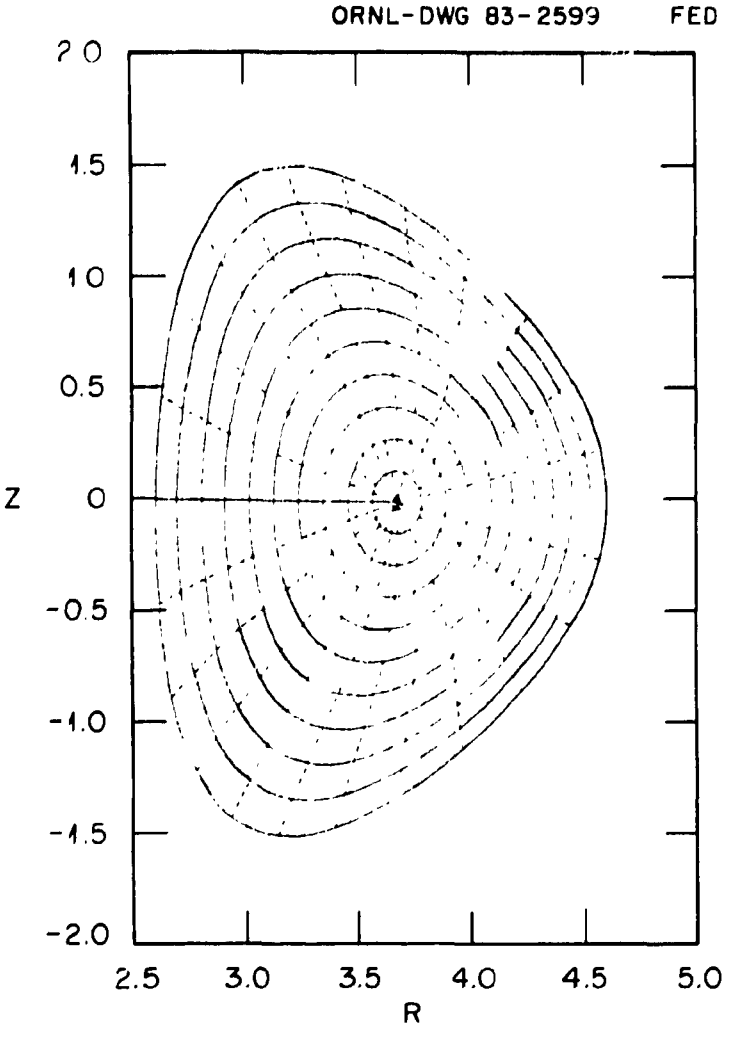

Fig. 5

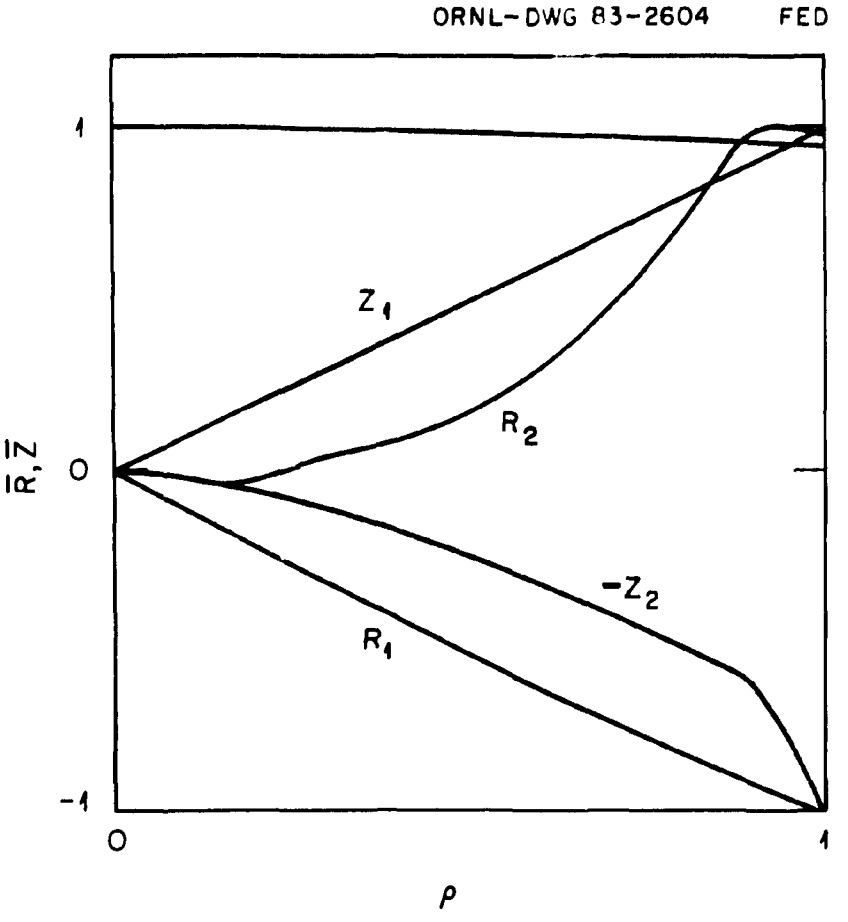

Fig. 6

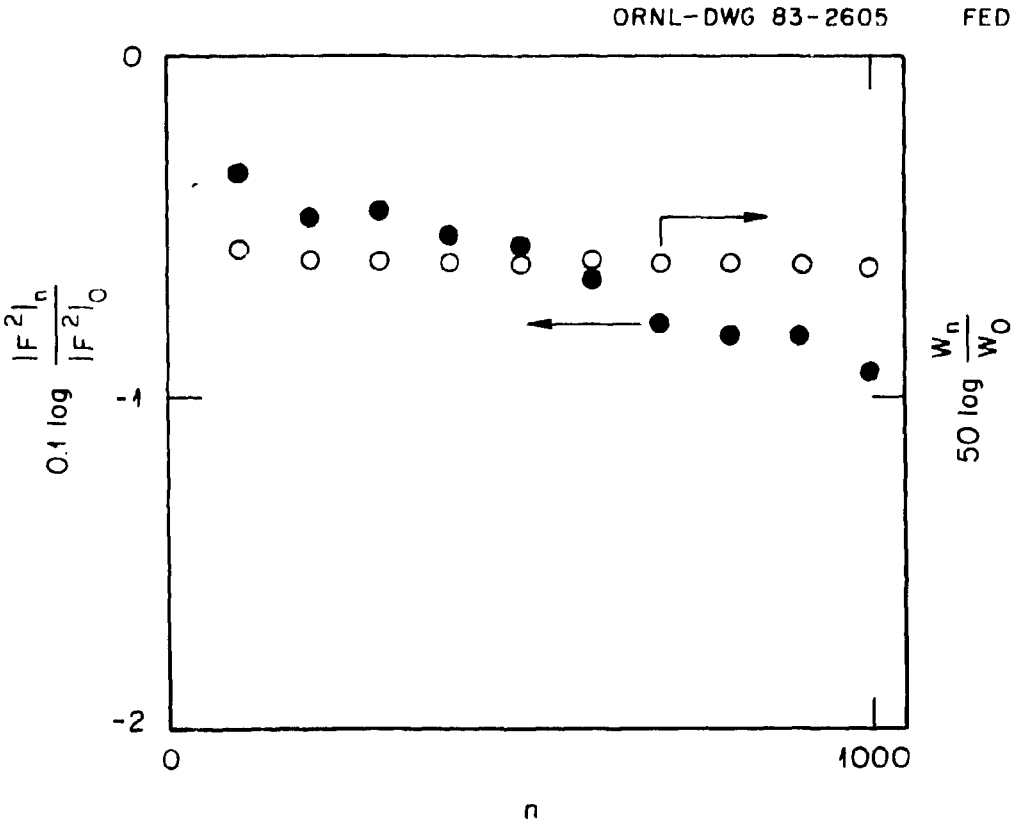

Fig. 7

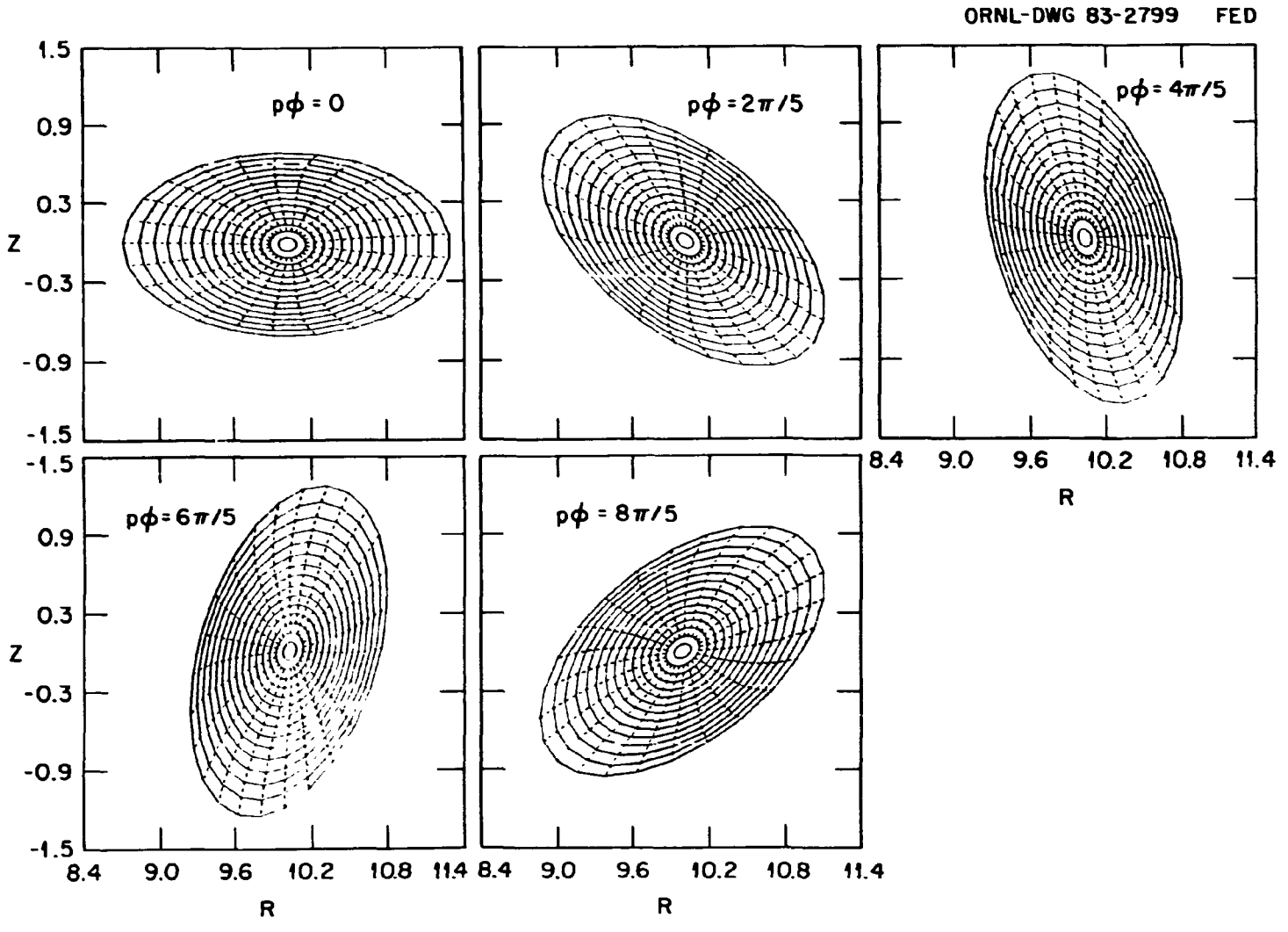
ORNL-DWG 83-2799 FED
pϕ = 0
pϕ = 2π/5
pϕ = 4π/5
pϕ = 6π/5
pϕ = 8π/5
Z
R
1.5
0.9
0.3
-0.3
-0.9
-1.5
8.4
9.0
9.6
10.2
10.8
11.4

Fig. 8

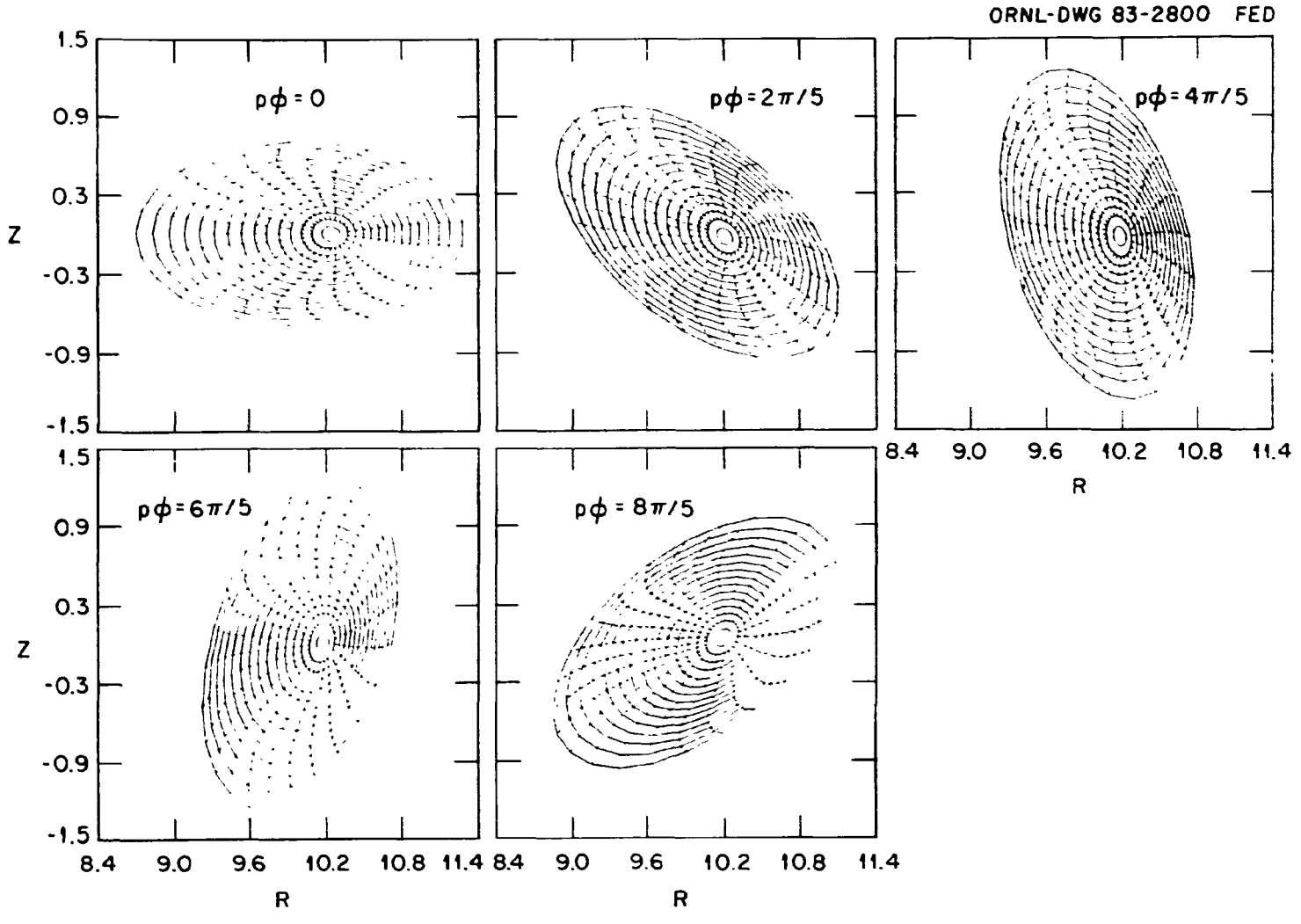
ORNL-DWG 83-2800 FED
pφ = 0
pφ = 2π/5
pφ = 4π/5
pφ = 6π/5
pφ = 8π/5
Z
R
1.5
0.9
0.3
-0.3
-0.9
-1.5
8.4
9.0
9.6
10.2
10.8
11.4

Fig. 9

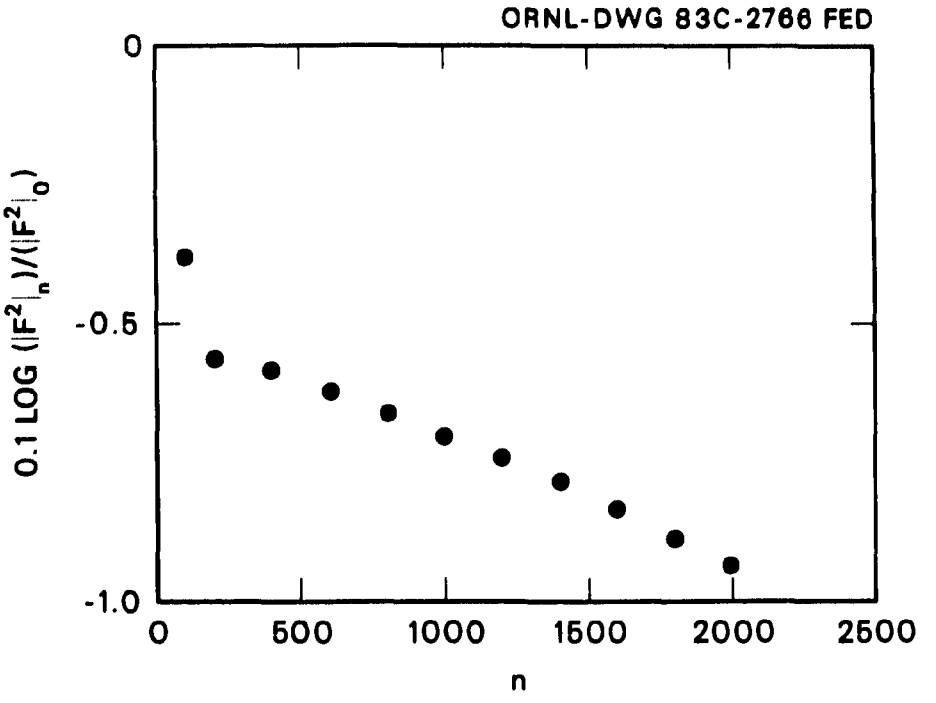
ORNL-DWG 83C-2766 FED
0
-0.5
-1.0
0.1 LOG (|F²|n)/(|F²|o)
0
500
1000
1500
2000
2500
n

Fig. 10

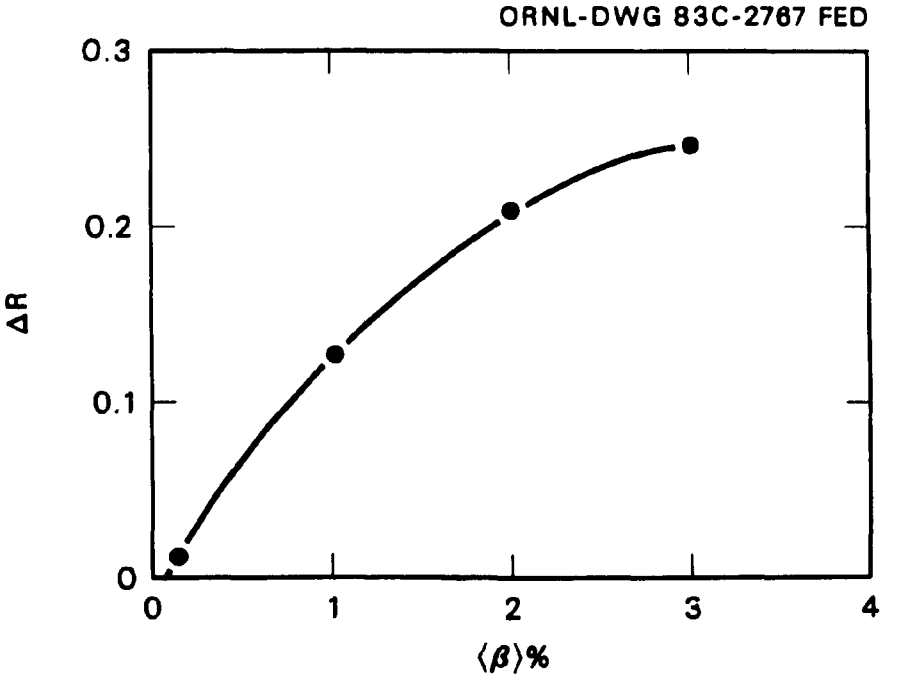
ORNL-DWG 83C-2767 FED
0.3
0.2
0.1
0
ΔR
0
1
2
3
4
⟨β⟩%

Fig. 11

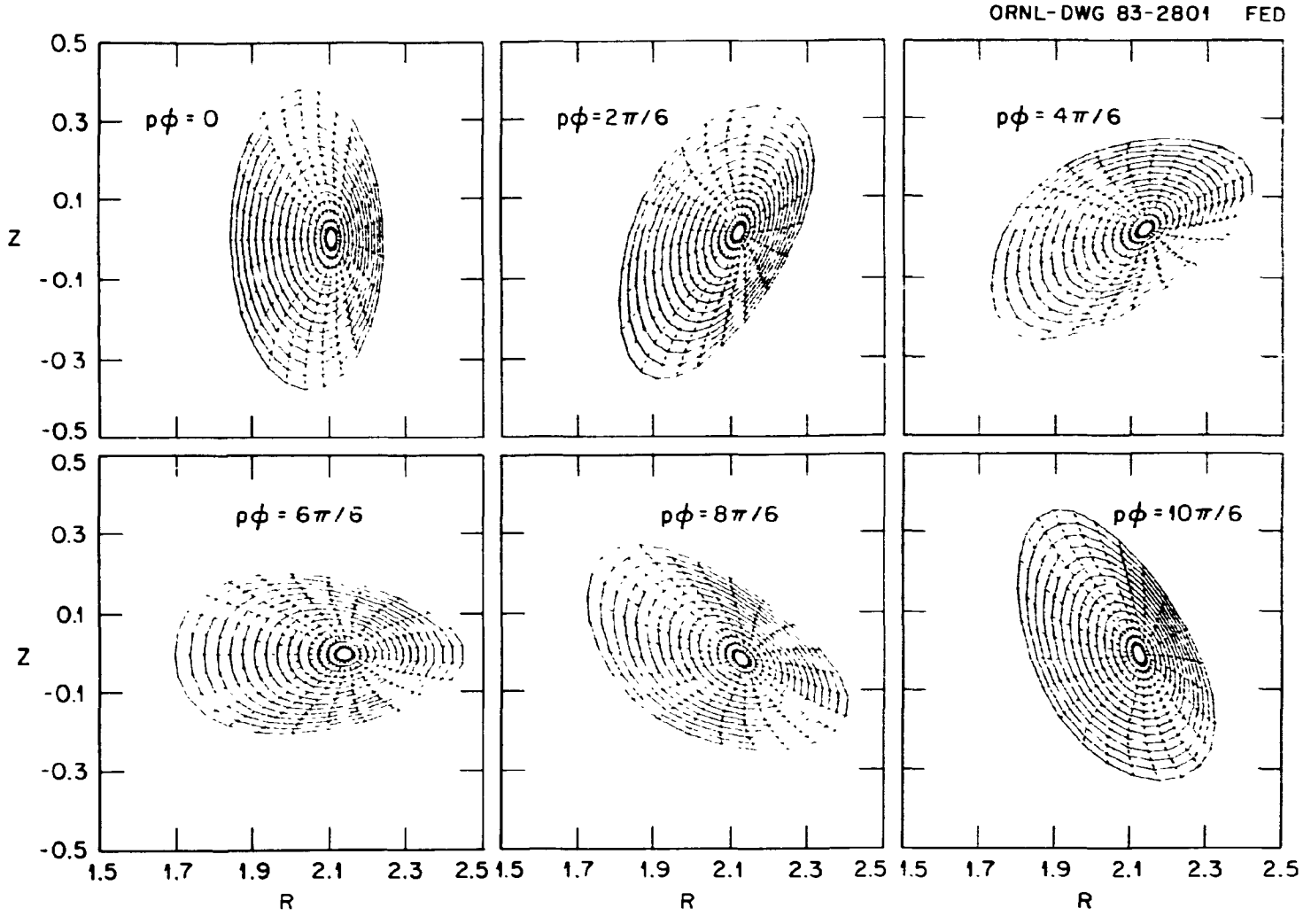
ORNL-DWG 83-2801 FED
pφ = 0
pφ=2π/6
pφ = 4π/6
pφ = 6π/6
pφ = 8π/6
pφ = 10π/6
Z
R
0.5
0.3
0.1
-0.1
-0.3
-0.5
1.5
1.7
1.9
2.1
2.3
2.5

Fig. 12

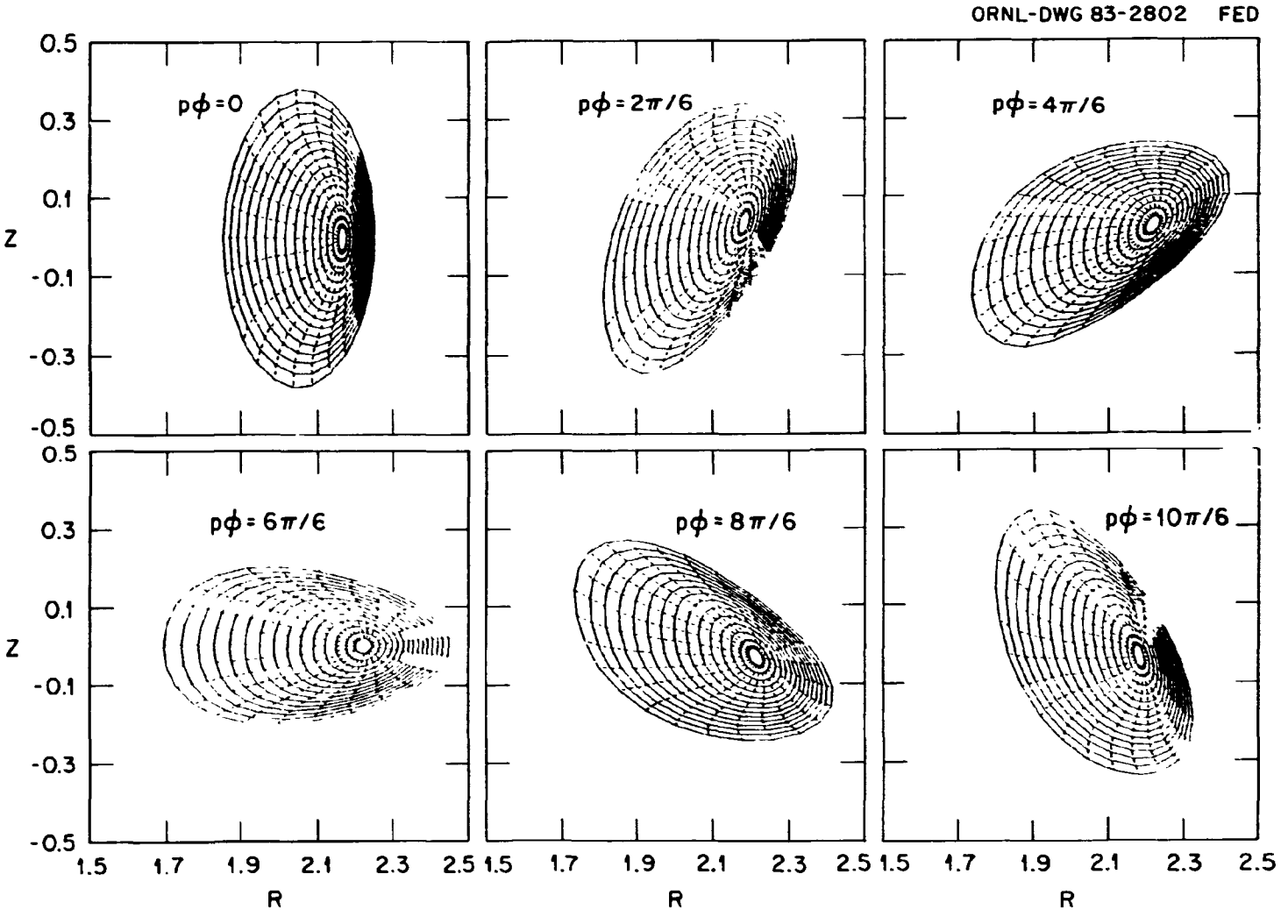
ORNL-DWG 83-2802 FED
pφ=0
pφ=2π/6
pφ=4π/6
pφ=6π/6
pφ=8π/6
pφ=10π/6
Z
R
0.5
0.3
0.1
-0.1
-0.3
-0.5
1.5
1.7
1.9
2.1
2.3
2.5

Fig. 13

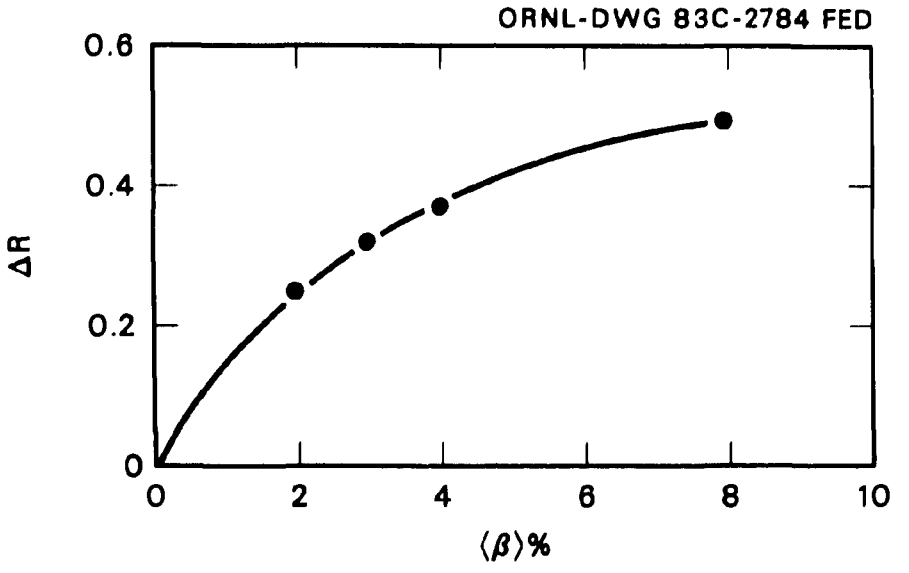

Fig. 14

ORNL/TM-8861
Dist. Category UC-20

INTERNAL DISTRIBUTION

1. S. E. Attenberger
2. L. A. Charlton
3. E. C. Crume, Jr.
4. R. A. Dory
5. J. L. Dunlap
6. R. H. Fowler
7. P. W. Gaffney
8. H. R. Hicks
9. J. A. Holmes
10. W. A. Houlberg
11. H. C. Howe
12. D. K. Lee
13. J. K. Munro, Jr.
14. M. Murakami
15. Y-K. M. Peng
16. J. A. Rome
17. D. J. Sigmar
18. C. E. Thomas
19. J. S. Tolliver
20. W. I. van Rij
21-22. S. P. Hirshman
23. J. C. Whitson
24-25. Laboratory Records Department
26. Laboratory Records, ORNL-RC
27. Document Reference Section
28. Central Research Library
29. Fusion Energy Division Library
30. Fusion Energy Division Reports Office
31. ORNL Patent Office

EXTERNAL DISTRIBUTION

32. Office of the Assistant Manager for Energy Research and Development, Department of Energy, Oak Ridge Operations Office, P. O. Box E, Oak Ridge, TN 37830
33. I. Bernstein, Yale University, New Haven, CT 06520
34. J. D. Callen, Department of Nuclear Engineering, University of Wisconsin, Madison, WI 53706
35. L. Chen, Princeton Plasma Physics Laboratory, P.O. Box 451, Princeton, NJ 08544
36. R. W. Conn, Department of Chemical, Nuclear, and Thermal Engineering, University of California, Los Angeles, CA 90024

37. S. O. Dean, Director, Fusion Energy Development, Science Applications, Inc., Gaithersburg, MD 20760
38. H. K. Forsen, Bechtel Group, Inc., Research Engineering, P. O. Box 3965, San Francisco, CA 94205
39. R. W. Gould, Department of Applied Physics, California Institute of Technology, Pasadena, CA 91125
40. D. G. McAlees, Exxon Nuclear Co., Inc., 777 106th Avenue, NE, Bellevue, WA 98009
41. P. J. Reardon, Princeton Plasma Physics Laboratory, P. O. Box 451, Princeton, NJ 08544
42. W. M. Stacey, School of Nuclear Engineering, Georgia Institute of Technology, Atlanta, GA 30332
43. G. A. Eliseev, I. V. Kurchatov Institute of Atomic Energy, P. O. Box 3402, 123182 Moscow, U.S.S.R.
44. V. A. Glukhikh, Scientific-Research Institute of Electro-Physical Apparatus, 188631 Leningrad, U.S.S.R.
45. I. Spighel, Lebedev Physical Institute, Leninsky Prospect 53, 117924 Moscow, U.S.S.R.
46. D. D. Ryutov, Institute of Nuclear Physics, Siberian Branch of the Academy of Sciences of the U.S.S.R., Sovetskaya St. 5, 630090 Novosibirsk, U.S.S.R.
47. V. T. Tolok, Kharkov Physical-Technical Institute, Academical St. 1, 310108 Kharkov, U.S.S.R.
48. R. Varma, Physical Research Laboratory, Navrangpura, Ahmedabad 380009, India
49. Bibliothek, Max-Planck Institut fur Plasmaphysik, D-8046 Garching bei Munchen, Federal Republic of Germany
50. Bibliothek, Institut fur Plasmaphysik, KFA, Postfach 1913, D-5170 Julich, Federal Republic of Germany
51. Bibliotheque, Centre des Recherches en Physique des Plasmas, 21 Avenue des Bains, 1007 Lausanne, Switzerland
52. Bibliotheque, Service du Confinement des Plasmas, CEA, B.P. No. 6, 92 Fontenay-aux-Roses (Seine), France

53. Documentation S.I.G.N., Departement de la Physique du Plasma et de la Fusion Controlee, Centre d'Etudes Nucleaires, B.P. 85, Centre du Tri, 38041 Cedex, Grenoble, France
54. Library, Culham Laboratory, UKAEA, Abingdon, Oxon, OX14 3DB, England
55. Library, FOM-Instituut voor Plasma-Fysica, Rijnhuizen, Jutphaas, The Netherlands
56. Library, Institute of Physics, Academia Sinica, Beijing, Peoples Republic of China
57. Library, Institute of Plasma Physics, Nagoya University, Nagoya, Japan
58. Library, International Centre for Theoretical Physics, Trieste, Italy
59. Library, Laboratorio Gas Ionizatti, Frascati, Italy
60. Library, Plasma Physics Laboratory, Kyoto University, Gokasho Uji, Kyoto, Japan
61. Plasma Research Laboratory, Australian National University, P.O. Box 4, Canberra, A.C.T. 2000, Australia
62. Thermonuclear Library, Japan Atomic Energy Research Institute, Tokai, Naka, Ibaraki, Japan
63. J. F. Clarke, Director, Office of Fusion Energy, Office of Energy Research, Mail Stop G-256, U.S. Department of Energy, Washington, DC 20545
64. D. B. Nelson, Acting Director, Division of Applied Plasma Physics, Office of Fusion Energy, Office of Energy Research, Mail Stop G-256, U.S. Department of Energy, Washington, DC 20545
65. W. Sadowski, Fusion Theory and Computer Services Branch, Office of Fusion Energy, Office of Energy Research, Mail Stop G-256, U.S. Department of Energy, Washington, DC 20545
66. N. A. Davies, Tokamak Systems Branch, Office of Fusion Energy, Office of Energy Research, Mail Stop G-256, U.S. Department of Energy, Washington, DC 20545
67. E. Oktay, Tokamak Systems Branch, Office of Fusion Energy, Office of Energy Research, Mail Stop G-256, U.S. Department of Energy, Washington, DC 20545

68. A. Bers, 38-260, Massachusetts Institute of Technology, Cambridge, MA 02139
69. O. Betancourt, Courant Institute of Mathematical Sciences, New York University, 251 Mercer Street, New York, NY 10012
70. H. M. Chen, Physics Department, University of Maryland, College Park, MD 20742
71. J. Corday, Culham Laboratory, UKAEA Research Group, Abingdon, Oxon OX14 3DB, England
72. J. DeLucia, Princeton Plasma Physics Laboratory, P.O. Box 451, Princeton, N. 08544
73. P. Garabedian, Courant Institute of Mathematical Sciences, New York University, 251 Mercer Street, New York, NY 10012
74. H. Goedbloed, Plasma Fusion Center, NW 16-243, Massachusetts Institute of Technology, Cambridge, MA 02139
75. H. Grad, Magnets-Fluid Dynamics Division, Courant Institute of Mathematical Sciences, New York University, 251 Mercer Street, New York, NY 10012
76. J. M. Greene, GA Technologies, Inc., San Diego, CA 92138
77. L. Hall, L-630, Lawrence Livermore National Laboratory, P.O. Box 5511, Livermore, CA 94550
78. L. Ibanez, Courant Institute of Mathematical Sciences, New York University, 251 Mercer Street, New York, NY 10012
79. J. C. Jardin, Princeton Plasma Physics Laboratory, P.O. Box 451, Princeton, NJ 08544
80. W. Kerner, Courant Institute of Mathematical Sciences, New York University, 251 Mercer Street, New York, NY 10012
81. L. L. Lao, TO-512, GA Technologies, Inc., San Diego, CA 92138
82. K. M. Liang, Princeton Plasma Physics Laboratory, P.O. Box 451, Princeton, NJ 08544
83. R. McCall, Princeton Plasma Physics Laboratory, P.O. Box 451, Princeton, NJ 08544
84. B. Miner, Science Applications, Inc., 1710 Goodridge Drive, McLean, VA 22102
85. R. Morris, Department of Nuclear Engineering, Georgia Institute of Technology, Atlanta, GA 30332

86. R. W. Moses, MS 642, Los Alamos National Laboratory, Los Alamos, NM 87545
87. H. Mynick, ECE Department, University of Wisconsin, Madison, WI 53706
88. A. Riedel, Courant Institute of Mathematical Sciences, New York University, 251 Mercer Street, New York, NY 10012
89. M. N. Rosenbluth, Institute of Fusion Studies, RLM 11.222, University of Texas, Austin, TX 78712
90. P. H. Rutherford, Princeton Plasma Physics Laboratory, P.O. Box 451, Princeton, NJ 08544
91. A. G. Sgro, Los Alamos National Laboratory, Los Alamos, NM 87545
92. A. Schluter, c/o A. Boozer, Princeton Plasma Physics Laboratory, P.O. Box 451, Princeton, NJ 08544
93. V. D. Shafranov, I. V. Kurchatov Institute of Atomic Energy, P.O. Box 3042, 123182 Moscow, U.S.S.R.
94. J. L. Shohet, Stellarator-Torsatron Laboratory, University of Wisconsin, Madison, WI 53706
95. A. M. M. Todd, Grumman Aerospace Corporation, 105 College Road East, Princeton, NJ 08540
96. Y. M. Treve, 125 San Rafael Avenue, Santa Barbara, CA 93109
97. J. W. Van Dam, Institute of Fusion Studies, RLM 11.222, University of Texas, Austin, TX 78712
98. H. Weitzner, Courant Institute of Mathematical Sciences, New York University, 251 Mercer Street, New York, NY 10012
99. J. C. Wiley, Institute of Fusion Studies, RLM 11.222, University of Texas, Austin, TX 78712
100. S. C. Jardin, Princeton Plasma Physics Laboratory, P.O. Box 451, Princeton, NJ 08544

101–208. Given distribution as shown in TID-4500, Magnetic Fusion Energy (Distribution Category UC-20)